Master's Thesis in Graduate School of Library, Information and Media Studies

Generation of airborne speakers using laser-induced breakdown

March 2020

201821618

Sato Yuta

Generation of airborne speakers using laser-induced breakdown

Sato Yuta

Graduate School of Library,
Information and Media Studies
University of Tsukuba

March 2020

Contents

List of Figures

Chapter 1

Introduction

The technique of generating plasma in both solid and liquid media using a high-power pulsed laser is well known. The LIB generated by pulsed lasers can reach temperatures of a 1,000 K in just a few hundred ns to a few ns. [1] Its high impulsivity creates a broad band of light, including X-rays and terahertz waves, and a shock wave (N-wave) like a sonic wave [2, 3]. This phenomenon is utilized in various ways, including non-thermal processing, stereoscopic displays, and X-ray light sources. [4, 5]

While there are many researches focused on the properties of light and heat, LIB is also attracting attention as a sound source with ideal sound source characteristics because it has a shape close to a true sphere and does not have a physical diaphragm to propagate sound. In previous studies, there were papers that measured LIB directivity and frequency characteristics [6, 2] and papers that treated LIB as an impulse sound source or shock wave source [7]. Their studie has shown that LIB can be used as a massless, non-directional, impulsive sound source. High-voltage air discharge phenomena, such as those represented by Tesla coils, have similar acoustic characteristics. Speakers using electric discharge have already existed and have been commercialized. In other words, it is possible to reproduce arbitrary waveforms in the similar way in LIB.

When sound is reproduced using electric discharge, there are physically unstable elements such as the distance between electrodes, vibration of electrodes, and oxidation of electrodes. On the other hand, LIB generates discharge by concentrating light in the air, so that physical equipment and sound sources can be completely separated. Therefore, reproducing an arbitrary waveform with LIB has an advantage in terms of repeatability over conventional methods applying electric discharge.

The technique of exciting sound waves using lasers is used in the field of photoacoustics, and has been applied to photographing images with high signal-to-noise ratio (SNR) in body photography, etc. In 2019, an experiment was conducted in which an infrared laser was driven into water vapor in the air to generate sound by photoacoustic effects [8]. This technique can be achieved using only a 100 mW/cm^2 laser power, so it is safer than LIB. However, as a characteristic of a sound source, it is difficult to have it for acoustic measurement because it has a radial directivity, and it is necessary to spray a medium that easily absorbs light into the gas.

LIB have attracted attention as a sound source that potentially satisfies ISO 3382-1 requirements, and many experiments have been conducted to measure directivity and impulse responses. The sound generated by LIB contains nonlinearity and propagates as a shock

wave [7]. Hosoya et al. experimentally verified the directivity of the sound source, focal length of the lenses, and sound pressure correlations, and measured the resonant mode frequencies of aluminum pipes using LIB [6]. Javier et al. generated LIB and measured Room Impulse Response [9]. This experiment showed that the LIB is massless because the reflection from the sound source cannot be confirmed. Such experiments show that the LIB has characteristics similar to an ideal point source with massless and omnidirectionnal.

Although previous studies have used LIB as a pure impulse sound source, actual RIR measurements use signals such as Maximum Length Sequance(MLS) [10] and Swept-Sine signal [11, 12]. Each of these is an impulsive noise or frequency sweep signal. Measuring the impulse response without using these signals reduces the SNR of the frequency response because of the lower energy at each frequency. Measuring impulse response in previous studies using LIB has been done used simple impulse signals because there was no way to play these signals. In this study, I focused on proposing a method for reproducing arbitrary waveforms in the audible frequency range in LIB. By sending a laser shutter signal to a sound source file that is pulse-modulated by Pulse Frequency Modulation (PFM)[13], the sound source can be played back electrically. The experiment focused on measuring the acoustic characteristics of the audible range that was played back. Since the equipment required to oscillate the laser generates a large amount of noise, I created a self-made anechoic chamber to perform measurements with high SNR and performed measurements while suppressing noise. From the results, I considered the characteristics of the sound source and the cause of the noise, and presented an application where this technology can be expected to be applied in the future.

Chapter 2

Theory

Physical phenomena used in this study are explained using figures. The necessary prerequisite knowledge is mainly knowledge of nonlinear optical phenomena and nonlinear acoustic phenomena. First, I explain the principle of LIB generation by a pulsed laser.

2.1 Optical background theory

2.1.1 Ionization

A high-intensity pulsed laser propagates while pushing away electrons in the air by a ponderomotive force. This force causes phenomena such as laser plasma acceleration to vibrate electrons, [14], tunnel ionization as described in this section, and so on.

Ponderomotive force is a nonlinear potential force that charged particles feel in an oscillating electromagnetic field, and the direction of the force is constant regardless of the polarity of the charged particle. Electrons are restrained by coulomb and Van der Waals forces. If electrons are ejected from this constraint, causing the molecule to be positively charged. This phenomenon is called tunneling ionization, and the energy required for tunneling ionization is more than 10^{14} W/cm^2 [15]. Ponderomotive force interferes with the potential force that binds the electrons, thereby disrupting the balance of potential energies. As a result, tunneling occurs when a weak part of the electron binding force appears. The ionized molecule pulls the electrons back and returns to a stable state, and the difference in energy held by the attracted electrons is excited as light. This sequence of flows is shown in Fig.2.1.

The electrons do not actually exist in a stopped state and oscillate somewhere between the potential barriers. Its presence probability is represented by a wave function. In visible wave motion, attenuation and reflection are eliminated when reflected at the wall, but quantum wave functions are not completely reflected and are known to seep out of the potential barrier. If the potential barrier is sufficiently thick, the reflection will be successful. However, if the barrier is thin, there is a chance that electrons will be projected outside the barrier. An electron constrained by a potential barrier passes through a thin part of the barrier caused by the ponderomotive force without reflecting, as shown in Fig.2.1. This phenomenon is called tunneling, because it seems that a tunnel opened in the barrier and electrons popped out. In Fig.2.1, the laser pulses are injected from the left side, and (a) to (c) in the figure are arranged in order of time.

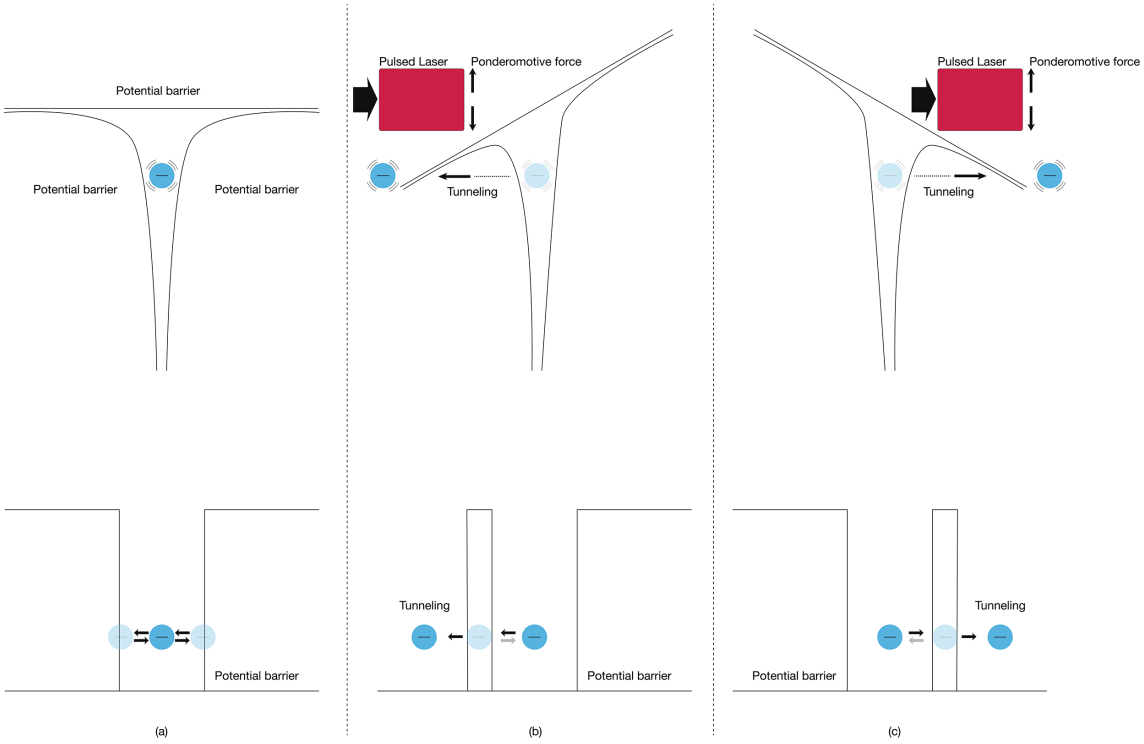

Figure 2.1: Potential fields that constrain electrons are changed by the incidence of a pulsed laser, and tunneling occurs.(a) Stable condition before laser passage.The electron is constrained by the well-type potential.(b) A state in which the laser enters from the left side and the potential field is changed by the ponderomotive force, and one side of the potential barrier which restrains the electron is thinned.(c) Likewise, the laser passes through and the potential barrier on the opposite side is thinned.

The wavelength of the excited light is determined by the energy of the electron. Excitation of light by photon absorption like fluorescence can excite a specific wavelength [16], but the plasma excited by tunneling in the atmosphere becomes white.

2.1.2 filamentation

High-power pulsed lasers propagate nonlinearly through the medium. Among the phenomena caused by the nonlinear self-action is the self-focusing effect, which affects the shape of the generated plasma. [17]

As the laser intensity increases, the refractive index of the air varies with the Kerr effect [18, 19, 20, 21]: $n = n_0 + n_2 * I$, where I is the incident intensity. In a Gaussian beam, the intensity decreases from the center to the edge, so that the refractive index at the center of the beam is greater than that at the edge. Therefore, in addition to the diffraction of the lens, the air itself acts like a lens (called "Kerr lens). Initially, this focuses the beam before the focal point of the lens, and ionized air produces a plasma. Second, when the intensity decreases and the production of the plasma stops, it diffuses due to the influence of plasma defocusing [22]. Then, the Kerr effect focuses the laser (Kerr re-focusing). Dynamic balance of Kerr effect and plasma non-convergence forms a stable structure composed of multiple plasmas called "filaments". [23, 24] This results in an elongated tail-shaped plasma.Fig.2.2 shown this phenomenon. It is predicted that a plasma with an extended tail due to fil-

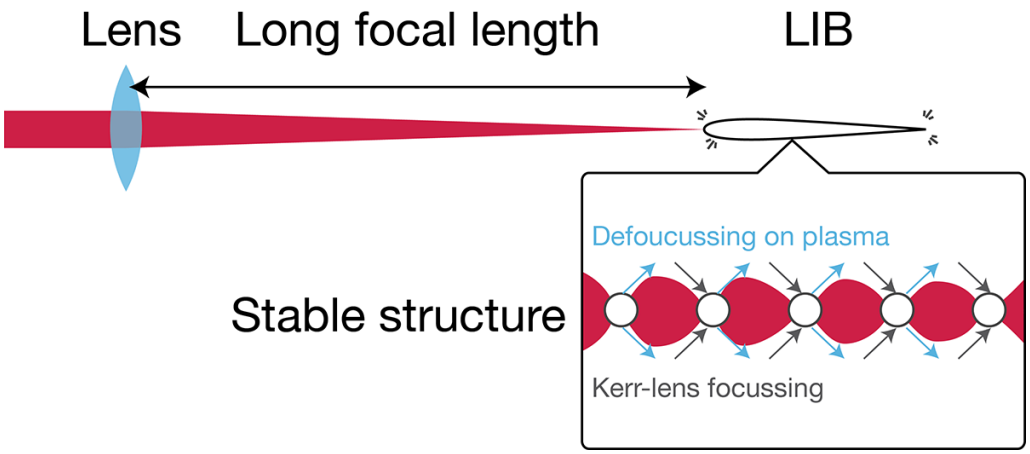

Figure 2.2: Defocusing in the plasma and self-reforcusing by the car lens are generated continuously, and plsma of multiple points is generated.

amentation will affect the directivity of the sound generated from the LIB as well as the directivity changes due to the path of the electric discharge.

The length of the plasma tail due to filamentation becomes longer for lenses with a longer focal length.

Since this study uses a lens with a focal length of 6mm, the effect is negligible.

2.1.3 Spot size

Since the laser irradiance must be kept high in order to promote ionization, a circuit design considering the spot size when the beam is focused is necessary. Ideally, it should be focused to an infinitesimal size, but the smallest spot size is limited by the diffraction limit.

A laser whose intensity distribution follows a Gaussian distribution has the same phase throughout the wavefront and propagates as a Gaussian beam after passing through the near-and far-field and optical systems. Therefore, the Gaussian beam can achieve the smallest spot size on the order of the wavelength of light.

The smallest spot diameter w_f when focusing a lens beam of focal length f is expressed by the product of focal length and divergence angle θ.[25]

$$w_f = f\theta, \tag{2.1}$$

Considering the diffraction limits, the divergence angle is expressed by

$$\theta = \lambda / w_0, \tag{2.2}$$

where w_0 is the diameter of the beam entering the lens, λ is the wavelength. Therefore, from Eq.2.1, the spot diameter is given by using the focal length, wavelength, and incident beam diameter.

$$w_f = f\lambda / w_0. \tag{2.3}$$

Depth of focus w_d is calculated using the geometric ratio between beam diameter and focal length as The depth of focus is expressed as

$$w_d = \lambda \frac{f^2}{(\frac{w_0}{2})^2} = 4\lambda \frac{f^2}{w_0^2}, \tag{2.4}$$

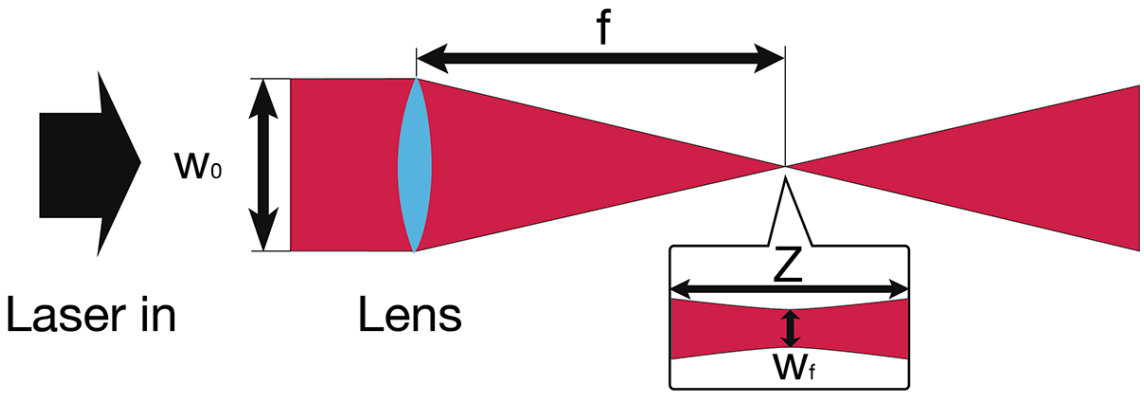

Figure 2.3: Visual comprehension of the parameters needed to calculate the focal diameter

using the geometric ratio of beam diameter to focal length, and the depth of focus w_0:w_f=f:$w_d/2$. The parameters in these equations are shown in 2.3 for a visual comprehension.

Regarding the spec sheet of objective lens, which combines multiple lenses to increase the numerical aperture, the spot size is stated in the data sheet published by the lens seller, and that value is used for the calculation.

2.2 Acoustic background theory

2.2.1 Nonlinear acoustic effect

LIB and electric plasmas raise the ambient temperature to thousands of kelvins during only a few nano second. This causes the air around the plasma to expand rapidly and propagate through a sparse wave [7]. Sound waves propagate through a variety of media, but this section describes air as a representative. Sound waves propagate as a sparse wave when air is compressed and expanded repeatedly. Air is viscous and the rate of compression and expansion is not equivalent. This is called nonlinearity, and acoustic phenomena generated by nonlinearity have been studied for a long time as nonlinear acoustics [26]. Nonlinearity is more pronounced because the amplitude of the sound wave increases and the higher the frequency, the faster the compression. For example, Don A. Webster et al. found that at 2kHz the sound pressure level begins to appear at 142dB and becomes clear at 148dB [27]. On the other hand, at an ultrasonic wave of 40kHz, nonlinearity already appears at 130dB [28, 29]. This principle is illustrated in Fig.2.4. When sound waves obey linear theory, the sound pressure level decreases by 6dB when the distance between the measurement point and the sound source is doubled from the inverse square law, but in nonlinear acoustics this rule is not true [9]. Sound waves with a large effect of nonlinear effects, such as Fig.2.4, are closer to the shape of a saw wave. Therefore, the propagation of a nonlinear sound wave is obtained by calculating it as the propagation of a saw wave [7]. The sound generated by LIB is strongly affected by the nonlinear effect near the generating point, but it attenuates according to the inverse square law when the distance is separated. Nonlinear effects can be minimized by controlling the laser source power even at neighboring points. [7, 6]

The attenuation of the sound pressure p due to the propagation distance of the saw wave

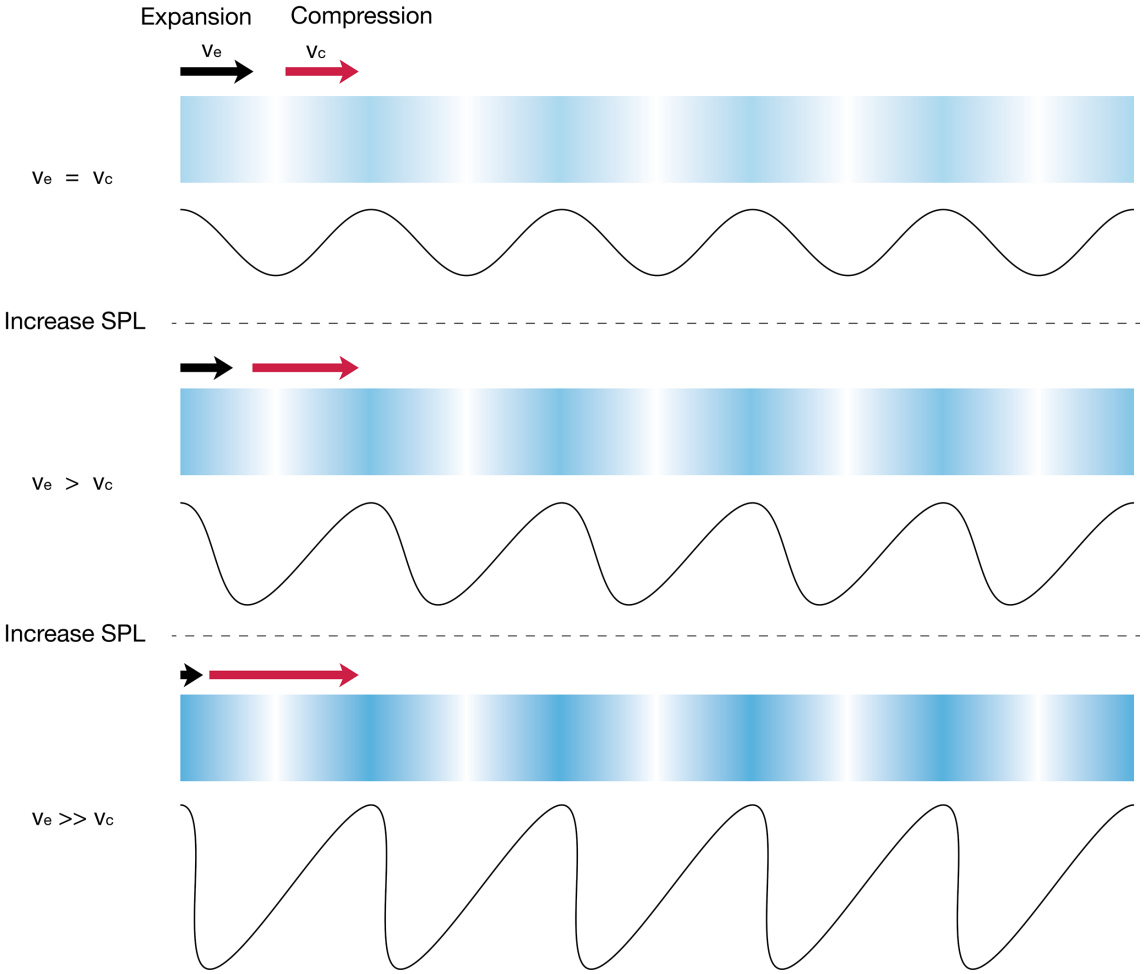

Figure 2.4: The process in which the amplitude of the sound wave rises and the difference between the compression velocity v_c and the expansion velocity v_e of the air increases, and the sine wave changes into a saw wave (N-Wave)

is expressed by the percentage of the increase of the pulse duration D as

$$\frac{D}{D_0} = \sqrt{1 + \frac{\epsilon p_0 x}{(c_0)^3 \rho_0 D_0}}, \tag{2.5}$$

$$D = D_0 \sqrt{1 + \frac{\epsilon p_0 x}{{c_0}^3 \rho_0 D_0}}, \tag{2.6}$$

$$p = \frac{p_0}{\sqrt{1 + \frac{\epsilon p_0 x}{(c_0)^3 \rho_0 D_0}}} = \frac{p_0 D_0}{D}, \tag{2.7}$$

where c_0 is the adiabatic sound velocity in air, ρ_0 is the density of air, and ϵ is the adiabatic constant, which is approximated by 1.2. D is the pulse width when propagating by distance x, and D_0 is the pulse width when x = 0. p is the sound pressure and p_0 is the sound pressure when x = 0. From Eq.2.7, it can be seen that the sound pressure of the shock wave propagates dispersedly in the time direction as the pulse energy also dispersedly.

Chapter 3

Related Works

3.1 Comparison of plasma characteristics

Plasma(LIB) is generated not only by laser but also by applying high voltage between electrodes. The characteristics of the two are very similar, so now talk about the differences with reference to previous research.

3.1.1 Electric discharge

Generation of plasma (electric discharge) by electrodes has been studied for a long time, and researchers who first discovered this phenomenon call this phenomenon [30]. Actually, electro discharges can be generate arbitrary waveforms (i.e. audio signal, chirp signal) which modulated by pulse width modulation (PWM) or pulse reputation frequency method [31, 32]. However, electric discharge has some drawbacks. [7, 2, 33]

1. There are every electric discharge have something difference, which are generated by temporary variations in breakdown potential, randomness of air-breakdown channels between electrodes, and vibration of electrodes.
2. The directivity varies with the distance between electrodes.
3. The electrode will oxidize.
4. Since the electrode must be installed in a plane or near a curved surface, reflected waves occur and interfere.

For directivity, the electric discharges generated from the electrodes are shown to be mathematically a diopole sound source [34]. However, the directivity varies depending on the distance between the electrodes. Furthermore, since the electrodes vibrate, fluctuations are likely to occur for each electric discharge.

In addition, the electric discharge itself does not reflect sound waves, but electrodes and other devices necessary for the generation of electric discharge reflect sound waves. Electric discharge does not separate the electrodes, so the electrodes reflects acoustic wave. To isolate this effect, a combination of a laser and a coil is necessary.

3.1.2 Laser induced breakdown

On the other hand, LIB has the following characteristics.

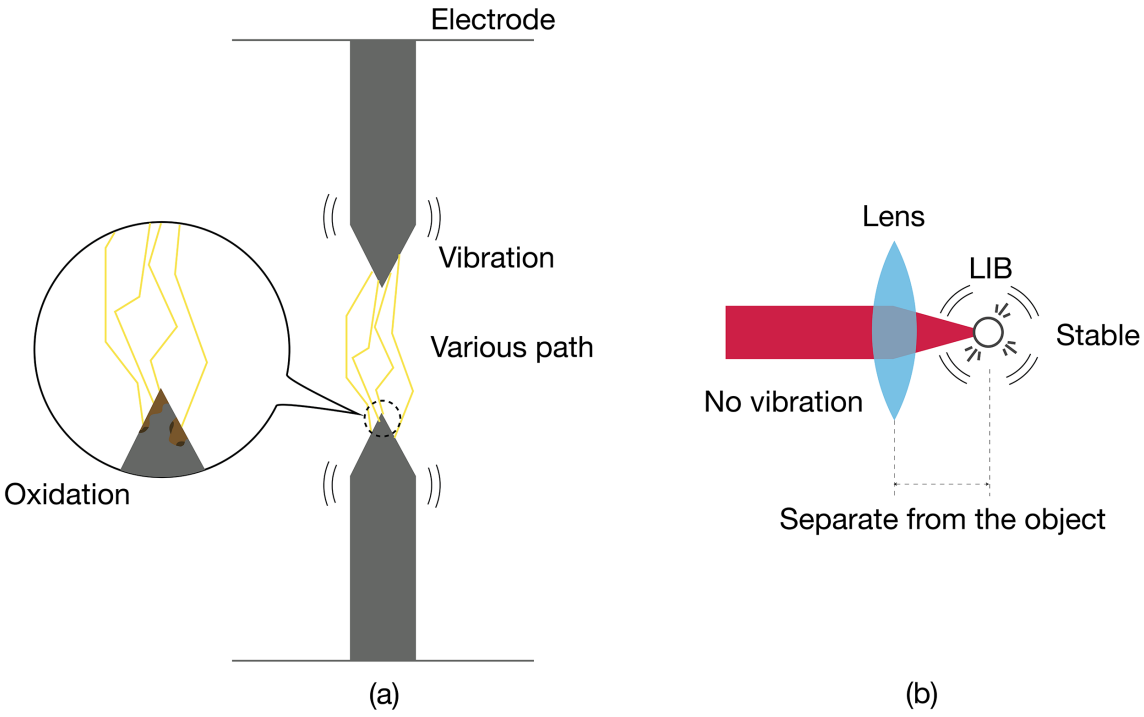

Figure 3.1: Comparison of elements related to the acoustic characteristics of electric discharge and LIB. (a) an electric discharge using electrodes (b) LIB produced by pulsed laser

1. LIB are generated from the point where the laser in the medium at focal point, if medium is gas, there are no objects that reflect sound other than the lens in the surrounding area.

2. Lenses can minimize acoustic interference by choosing an object with a long focal length.

3. Naoki Hosoya et al. have shown that the pulses of LIB are highly repeatable [6]. In other words, there is little fluctuation at each pulse.

4. LIB are massless sound sources.

In electric discharges, the directivity near the sound source is closer to the long sphere than the sphere, whereas in LIB, it is known that the directivity near the sound source is closer to the sphere [6, 2]. Caused LIB in a small space surrounded by glass, measured the impulse response of the space, and confirmed that there was no acoustic reflection from the sound source [35, 9]. Since no reflected sounds from other than the walls were observed, it can be read that there is no reflected sounds from the sound source, i.e. the LIB is massless source.

Comparison between LIB and electric discharge is summarized in Fig.3.1. Plasmas generated by both electricity and lasers emit sound to produce shock waves. This shock wave is called a N-wave because it resembles the alphabetic "N". Because it is significantly affected by air nonlinearity, its characteristics differ from those of ordinary sound waves.

3.2 Application to acoustic measurement

There are several studies focused on the acoustic characteristics of LIB. LIB has many acoustically superior characteristics as described in the comparison with electric discharge. Particular attention has been paid to the high repeatability and the high impulsivity of impulse response.

3.2.1 Measurement of room impulse response

Javier et al. measured the laboratory RIR by using LIB[9]. In its experiment, the result of the impulse response which obtained by the LIB is very short, so the peak of the impulse response is clear.

This experiment shows that the LIB is a massless sound source, because no acoustic reflection is observed from the LIB itself. Also, when the distance from the LIB is separated, the sound pressure is attenuated in proportion to the square of the distance, indicating that the measurement can be performed without being affected by nonlinearity.

3.2.2 Resonant mode analysis of open tube

Hosoya et al. generated LIB inside aluminium pipes to analyze vibrational modes in the pipes [6]. The resonant frequencies obtained from the results of generating LIB at points 27.6mm from the inlet of the tube were compared with the values calculated from the mathematical formulas for the resonant modes of the open tube, indicating that the error rate was less than 1% during the 1st to 8th. Since LIB does massless, it is a great advantage that even if a LIB is generated in the conduit, the object's sound characteristics are not affected.

However, when LIB is generated at a position 99mm from the entrance of the tube in this experiment, the vibration mode did not conform to the calculated value, and therefore, it is necessary to pay attention to the arrangement of the sound sources when conducting resonance experiments. It is expected that LIB will perform best when present in the area of standing waves.

Experiments on directivity have also been conducted, and it has been confirmed that the sound pressure distribution is uniform in all directions.

3.2.3 Directivity control by three-dimensional arrangement

Some researchers have focused on this very excellent directivity. The LIB also has the characteristic that it can be freely positioned in the air. Taking advantage of this, Eskelinen et al. experimentally demonstrated that directivity can be controlled by generating Volumetric array with multi-points LIB [36].

In order to control the directivity by arranging high-frequency oscillators in an array, it is necessary to arrange the oscillators according to the wavelength size. However, high-frequency oscillators have mechanical limitations because of their short wavelengths. However, if the directivity is controlled by the arrangement of multi-points LIB in this way, multi-points LIB can solve such constraints because they are very small.

3.2.4 Acoustic source for nonlinear acoustic experiments

In addition, since the waveforms of sound generated from LIB are N-wave, applications to simulations of shock waves in laboratories have been proposed as sound sources that generate shock waves from extremely small points [7].

In a paper by Qin et al., it was confirmed that the LIB can produce a sound pressure of 181dB with reference to 20μPa (the minimum sound pressure that human hearing can hear). Since this exceeds 140dB, it is sufficient sound pressure to generate a shock wave. In addition, the study examined the nonlinearity of LIB and showed that it was sufficiently possible to apply it to laboratory shock wave experiments. In order to reproduce an acoustic signal with these signals, it is necessary to modulating the acoustic signal.

3.3 Modulation of acoustic signal

The technique of transmitting information such as acoustic signals on radio waves by changing the frequency and amplitude of radio waves is applied to familiar equipment such as radios. Radio waves carrying information are called carrier waves. It is classified into analog modulation, digital modulation and pulse modulation according to the shape of the carrier wave. Typical analog modulations include amplitude modulation (AM) that modulates the amplitude of the carrier wave, and frequency modulation (FM) that modulates the frequency of the carrier wave. Ochyai proposes highly directional aerial speakers by reproducing AM-modulated acoustic signals with an ultrasonic phased array that focuses ultrasonic waves in the air [29]. Because the LIB is highly impulsive, the carrier wave is considered as a pulse wave. Olaf et al. use electrodes to generate a nanosecond repetitively pulsed (NRP) plasma and pulse-density-modulated (i.e. Pulse frequency modulation). Played low frequency acoustic signal [32]. This paper modulates the acoustic signal with pulse frequency modulation (PFM) [13].

Chapter 4

Implementation

This section describes the system used in this work. I will explain the laser speck, the modulation method of the sound source, and the control system.

4.1 System overview

The Fig.4.1 shows the setup of the system used in this paper. Laser shutters are controlled electrically by receiving signals from the Field programable gate array(FPGA). The FPGA is equipped with a CPU, and the CPU is operating at Linux OS(Ubuntu16. 04. 1 LTS).

The sound source file is pre-modulated by the program and stored in the CPU in text format.

The laser is focused in the atmosphere to excite the plasma. Used laser source is a femtosecond laser with a central wavelength of $1035nm$, a repetition friquency of $1k-1MHz$ and a maximum pulse energy of $40\mu J$. Table.4.1 shows the laser source specifications.

4.2 Laser source

In this paper, Monaco[1] 1035-40-40 femtosecond laser developed by Coherent Co. with a central wavelength of $1035nm$, a repetition friquency of $1k-1MHz$ and a maximum pulse energy of $40\mu J$ was used. Table.4.1 shows laser spec.

Pulse width is variable up to 275fs-10ps. To increase the instantaneous power of the pulse, the shortest pulse width of 275fs was used for the main. Note that laser peak intensity rather than pulse width is important for LIB generation [10]. When the diameter of the emitted beam is 2.7±0.3mm and condensed by the lens as it is, it is difficult to increase the energy to $10^{14}\mathrm{W}/cm^2$, which is necessary for the generation of LIB, unless a lens with a high numerical aperture (NA) is used.

The laser supports shutter control by external triggering of the 5V. In the setup, signals from the FPGA were input to the signal line marked "Gate" on the rear of the laser.

4.3 Optical circuit and component

The optical component required to generate LIB is a lens that focuses the laser beam to increase the laser power per unit area. Since the laser pulses required to reproduce the

[1] https://www.coherent.com/lasers/laser/monaco

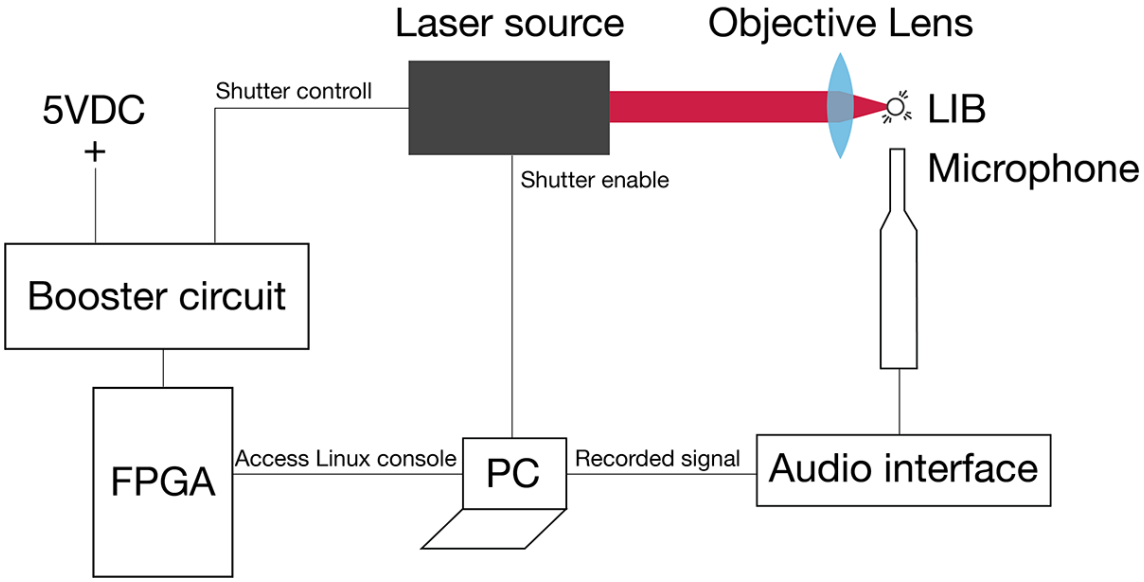

Figure 4.1: Overall system diagram. The FPGA controls the laser source and plays the sound by electrically controlling the internal shutter.

sound source are modulated electronically by the FPGA, optical circuits do not require any other components than lenses. Since the pulse energy of the laser is as small as 40 μJ, it was necessary to use a lens with a large aperture to generate LIB. The lens used in this paper is a THORLABS, Inc objective lens (LMH-20X-1064[2]) with a focal length (working distance) of 6mm and a numerical aperture of 0.40.

The energy density E W/cm^2 per hour of laser pulse is calculated by

$$E = \frac{E_{pulse}/t}{\pi r^2} = \frac{E_{pulse}}{\pi r^2 t}, \tag{4.1}$$

where E_{pulse} is the peak energy (J) of the laser pulse, t is the pulse width (s) of the laser pulse, and r is the laser spot diameter (cm^2). Since the peak power of the laser pulse is 40μJ, the pulse width is 275 fs, and the spot size of the lens is 2.5 μm, the pulse energy per unit area is 7.41×10^{14}W/cm^2. Since this value is above 10^{14}W/cm^2, it can be seen that enough energy is obtained for the generation of LIB.

A minimum spot size of 4.0μm is required to obtain energy in excess of 10^{14}W/cm^2 with the laser used in this paper. In order to obtain a focal diameter of 6.8μm from the Eq.2.3, the following equation can be obtained for the focal length of the lens and the incident beam diameter to the lens.

Table 4.1: Specifications of laser source.

Manufacturer	Coherent
Pulse duration	275 fs-10 ps
Pulse repetition friquency	1kHz≤1MHz
Maximum energy/pulse	40 μJ
Maximum time-averaged power	40 W
Beam diameter	2.7 ± 0.3 mm

[2]https://www.thorlabs.co.jp/thorproduct.cfm?partnumber=LMH-20X-1064

$$f = \frac{6.8w_0}{1035 * 10^{-3}} \approx 6.57w_0, \tag{4.2}$$

Therefore, for example, in order to generate plasma with a lens with a focal length of 10cm, the beam diameter should be increased to about 1.52cm. Since the optical system required for beam diameter conversion lengthens the pulse width of the laser, it is actually necessary to use a larger lens. In order to maximize the power of the sound source, this paper conducted an experiment using an objective lens. The height of the laser source exit is only 40mm. To avoid the effects of acoustic reflections from the optical platen, the laser was launched by a mirror to a height of approximately 200mm.

A mirror placed in the path of the beam attenuates the power of the laser beam according to the reflectivity. For example, a circuit using three 95% reflectivity mirrors eventually attenuates laser power to approximately 86%. In the experiment described in this paper, the mirror used a dielectric mirror[3] with a reflectivity of 99% or higher so as not to affect the power of the laser beam as much as possible.

4.4 Modulation of acoustic signal

The laser source operates at a repetition friquency of 1k-1MHz. By using an external trigger to control the shutter, you can determine timing at open or close the shutter at repetition frequencies. Therefore, I captured the carrier wave as a pulse wave and applied PFM to an acoustic signal whose sampling frequency was synchronized with the repetition frequency of the laser source. Fig.4.2 shows the relationship between the sampling frequency of the sound source and the repetition friquency of the laser source. An example of PFM implementation is as follow.

ALGORITHM 1: Pulse Frequency Modulation algorithm

Input: Wave file sampled at laser repetition friquency
Output: Pulse Frequency Modulation result on text file
while *Number of sample data* **do**
  sum ← sum +sample value; **if** sum > threshold **then**
    PFMvalue ← 1;
    sum ← sum-threshold;
  else
    PFMvalue ← 0;
  end
  go next sample;
end

The number of samples is calculated by multiplying the duration of the sound source by the sampling frequency. The Sample value is the amplitude of the samples, taking a between -1.0 and value of 1.0. In this paper, I normalized all sample values to 0 and modulated them by adding 1. The modulated sample sound is shown in Fig.4.3.

Now I explains how this modulation can reproduce an arbitrary waveform in LIB. The sound source file records amplitude values at regular intervals to represent analog waveforms digitally. The analog waveform is quantized by the number of bits and the sampling

[3]https://www.thorlabs.co.jp/thorproduct.cfm?partnumber=BB1-E03-10

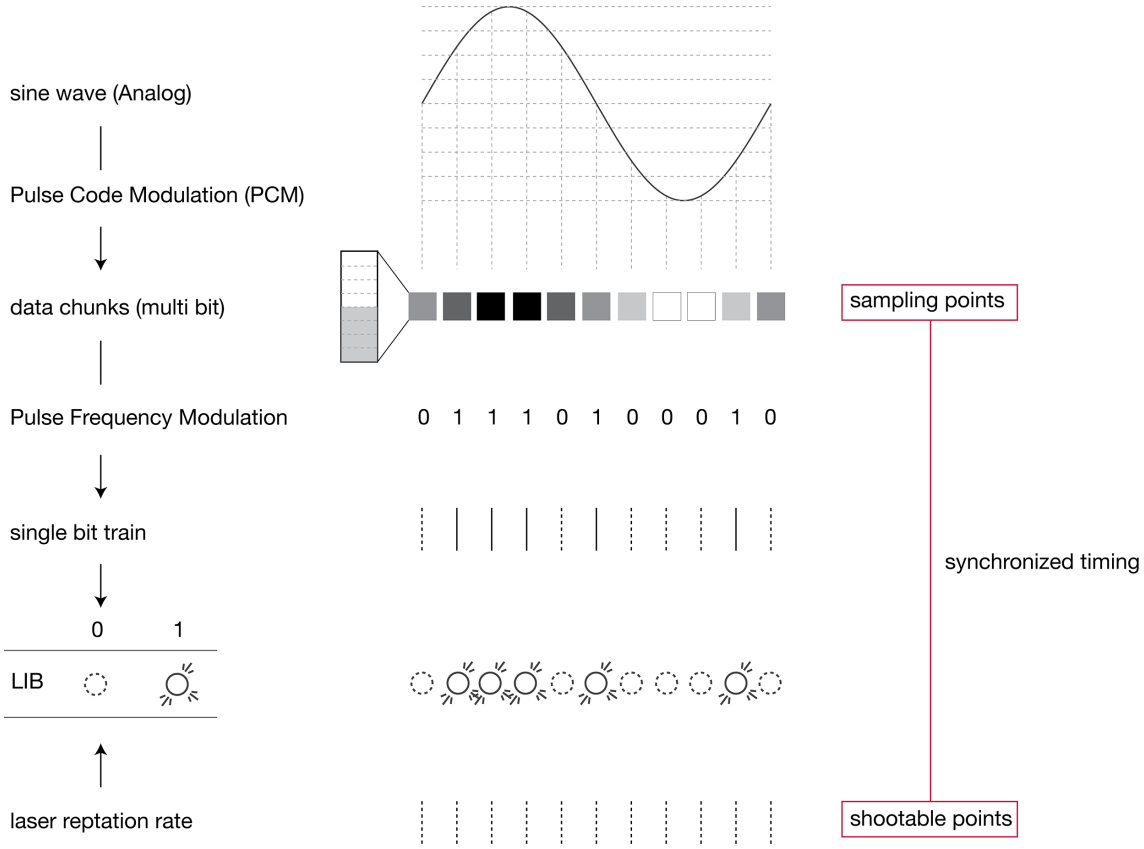

Figure 4.2: Relationship between the sampling frequency of the sound source and the repetition frequency of the laser. Describes the principle by which a sound source file can be reproduced by a laser.

frequency into parameters. The number of bits determines the resolution of the amplitude domain and the sampling frequency determines the resolution of the time domain. For example, if the bit rate is 16-bit sampling frequency is 40kHz, 40,000 pieces of data are represented in 16-bit per second.

Since the sampling frequency of the sound source file determines the time (timing) at which the data is quantized, it can be seen that the timing at which the PFM algorithm repeatedly adds (integrates) matches the sampling frequency. When the result of this integration exceeds the threshold, a pulse is generated. Therefore, the timing of generating the pulse by synchronizing the repetition frequency of the laser source with the sampling frequency of the sound source is synchronized with the result of the PFM.

4.5 Design of FPGA circuit

The shutter control of the laser source was performed using FPGA(DE1-SoC Board, Terasic Inc.[4]). The FPGA circuitry design is shown in Fig.4.4. The on-board CPU are operating at Linux OS(Ubuntu16.04.1 LTS), PFM-modulated acoustic signals which convert a binary file (i.e. pulse patterns) is stored in CPU beforehand. Data is sent to the FPGA by reading the binary and executing the program that outputs the data to the pins of the CPU on

[4]https://www.terasic.com.tw/cgi-bin/page/archive.pl?Language=English&No=836

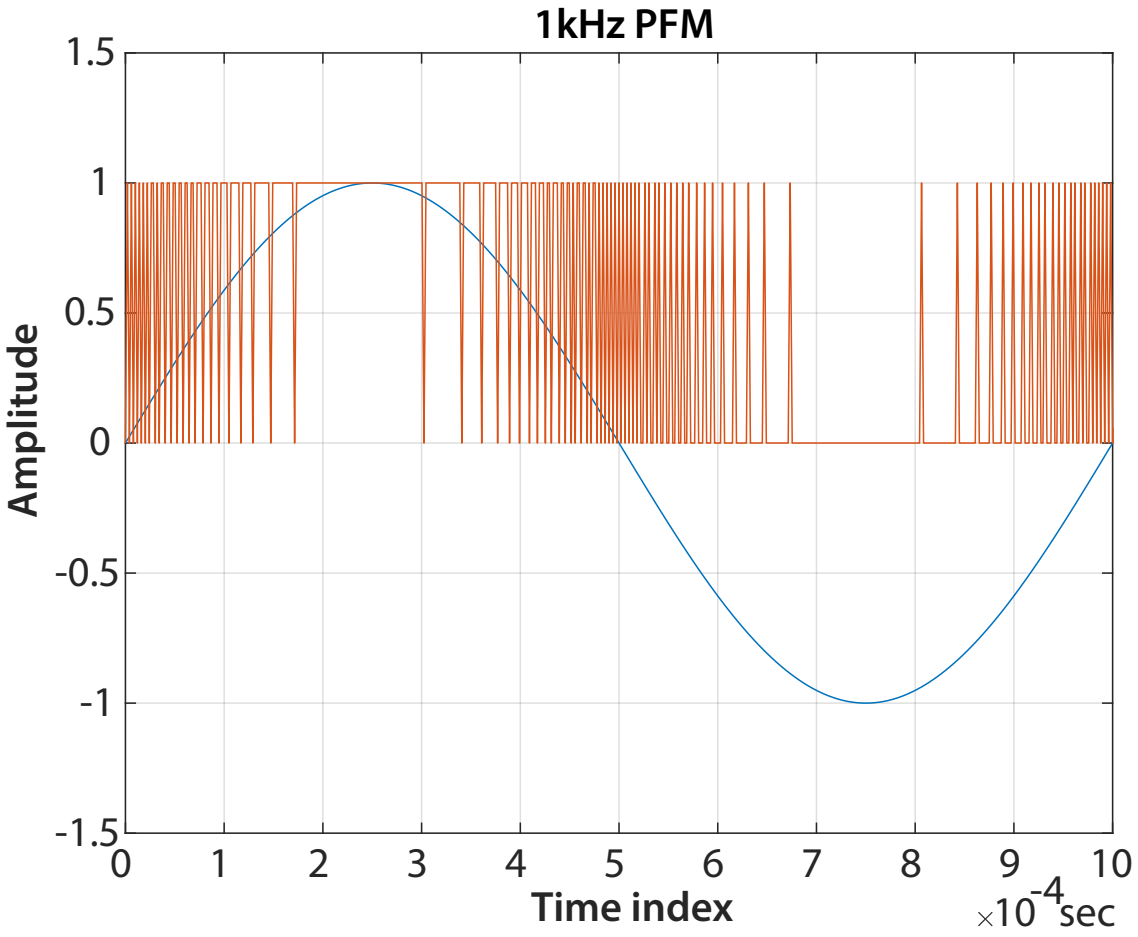

Figure 4.3: Example of converting a sine wave of 1kHz into a pulse pattern by PFM.

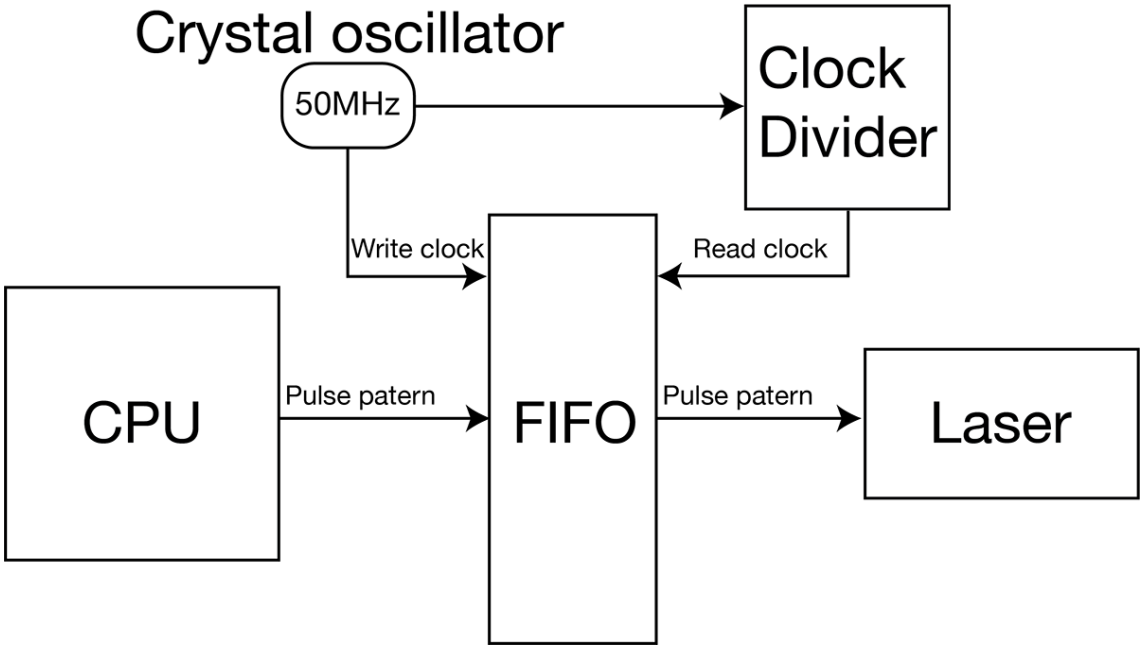

Figure 4.4: Modular schematic of the FPGA..

the Linux console. Data sent from the CPU is stored in the SLAM as a FIFO(First In First Out) cue. From this cue, it was read at a clock with the same frequency as the laser repetition frequency and output from the GPIO pins to control the laser shutter with the pulse pattern of the modulated sound source. The clock for reading from the FIFO must be divided from the system clock (50MHz), synchronize to the sampling frequency of the sound source.

Three different sampling frequencies are used in the experiments in this paper. Rewriting FPGA circuits take a long time, so the slide switches set the clock frequencies selector. It is necessary to design the counter by dividing the clock. However, if the output from the counter is used as a dividing clock as it is, the clock is generated at an unintentional timing, resulting in noise. Therefore, in the circuits designed in this paper, the output of the counters is connected to the ENABLE of the flip-flop with enable at the subsequent stage, so that the high is output when the ENABLE is high. In addition to this technique, there is also a ripple clock technique that achieves noise-free division by stacking multiple flip-flops whose output is inverted by the input of a clock. However, since the length of pulses, etc. can be changed, I adopted a method to prevent noises by using ENABLE for future expandability.

4.6 Booster circuit

Laser source gated by 5V signal. Since the voltage of the signals output from the FPGA is 3. 3V, the voltage is boosted to the 5V using an inverter (TC7WU04FU, TOSHIBA CORPORATION[5]). The circuit diagram is shown in 4.5, and the circuit actually created is shown in 4.6.

An inverter provides a function to invert the signal. The inverter used inverts the input

[5]http://akizukidenshi.com/download/ds/Toshiba/TC7WU04FK_datasheet_ja_20141118.pdf

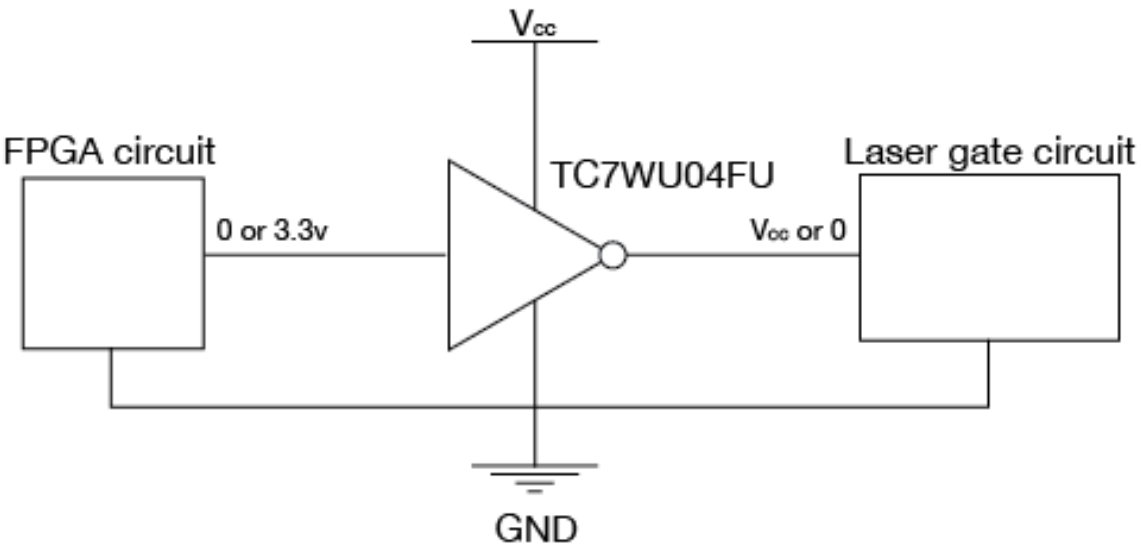

Figure 4.5: Electrical schematic of the booster circuit.

status (Hi or Low) to determine the output and outputs the voltage at the same value as the supplied power voltage. This allows the source signal to be boosted while inverting the signal, although the source signal is 3. 3V by turning the supplied power 5V. Since the device response speed is guaranteed to be 20ns or less in the power supply voltage 5V, the device can handle up to 50MHz of the maximum clock speed of the FPGA crystal resonator.

In order to make the circuit resistant to noise, the ground is widely connected by copper foil, and the connection distance from each signal line and power supply line to ground is designed to be short.

Signal inputs and outputs are made via coaxial cables using SMA connectors. The shielded cable prevents noise from entering the cable. Since the input is reversed by the inverter, the output from the FPGA is inverted and output, so the correct pattern is output. Fig.4.7 shows how the voltage of the signal is increased by boosting. Channel 2, represented by the blue line, shows the signal before boosting, and channel 1, represented by the yellow line, becomes the inverted signal after boosting.

4.7 Making a Chamber for acoustic measurements

In order to accurately evaluate the acoustic characteristics of the LIB, I assembled an anechoic chamber with a hole through which a laser can be injected, and used it for experiments. Photographs of the actually created chamber are shown in Fig.4.8. Various chamber parameters have been determined with reference to previous studies. This section describes how to determine each parameter.

4.7.1 Cutoff frequency of wedge

In order to accurately acquire the LIB sound, I created an anechoic chamber in which the inside was covered with a wedge-shaped sound absorbing material arranged in a checkerboard pattern, and used it for measurement.

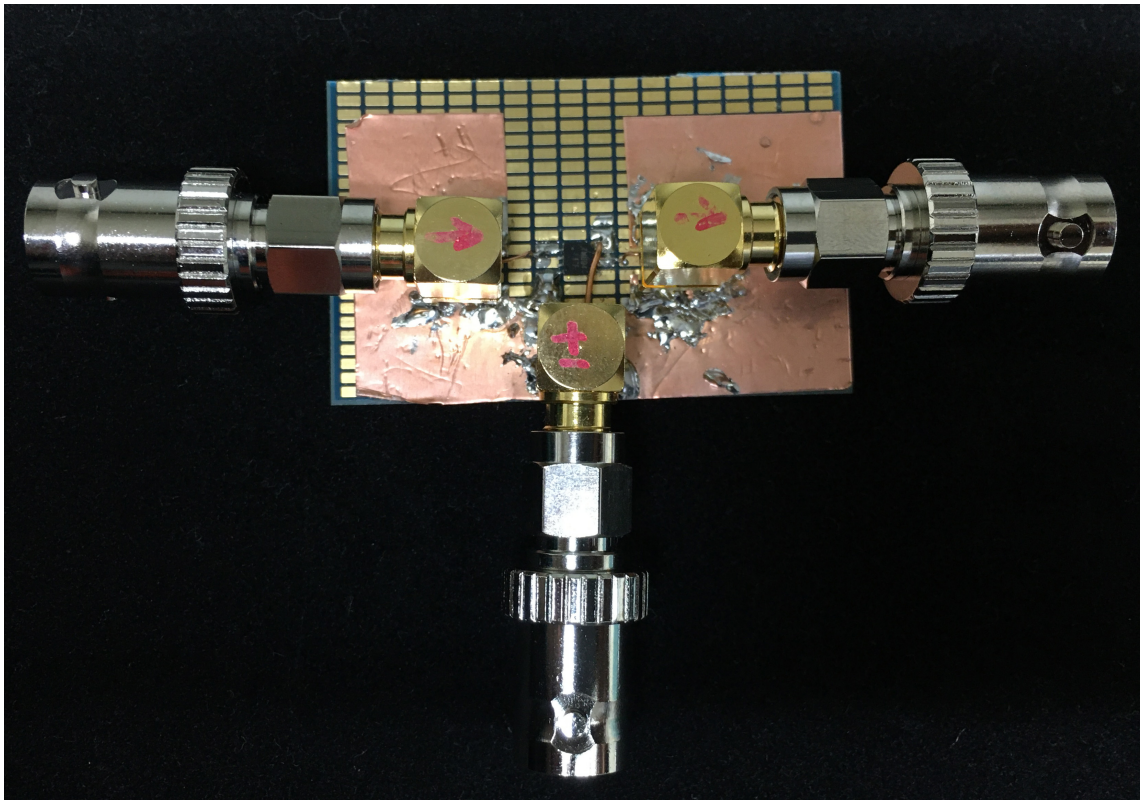

Figure 4.6: Photograph of the booster circuit. The voltage is boosted by the IC chip (inverter) in the center.

Due to the size of the surface plate, the size is limited, so the internal dimensions are designed to be a cubic shape with each side of 60cm. The cutoff frequency of a wedge is calculated from [37]

$$f_c = \frac{c}{4h}, \tag{4.3}$$

where fc is the cutoff frequency, c is the sound speed, and h is height of a wedge at the speed of sound. The chosen wedge[6] is 75mm high, and if the sound velocity c is 340m/s, the cutoff frequency is 1.13kHz.

4.7.2 Vibration isolator

The chamber is equipped with an anti-vibration mount to prevent vibration from the installation surface. The air damper WF4016 of Bridgestone Inc. was used. The material is a natural rubber type suitable for vibration-proof rubber classified as type A in JIS K 6386. From the spring constant of the rubber, the natural frequency f_0 (Hz) is obtained by [38]

$$f_0 = \frac{1}{2\pi}\sqrt{\frac{k}{m}} = \frac{1}{2\pi}\sqrt{\frac{kg}{W}}, \tag{4.4}$$

where k is the dynamic spring constant of rubber vibration isolator (N/mm) and is expressed by 1.2 times the static spring constant.

$$W = mg, \tag{4.5}$$

[6]https://www.sonorize.jp/urethane-parts

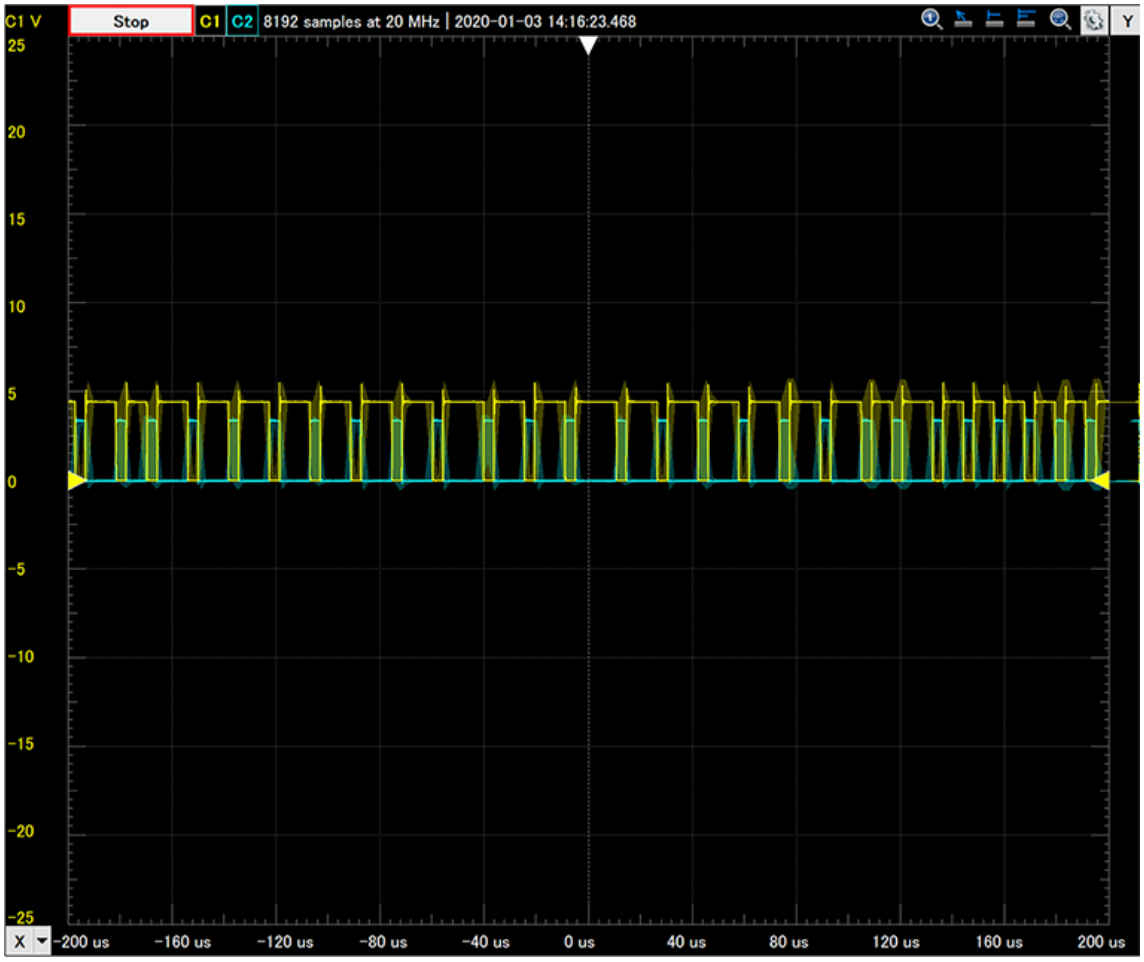

Figure 4.7: Input signal (blue line) and output signal (yellow line) to the booster circuit.

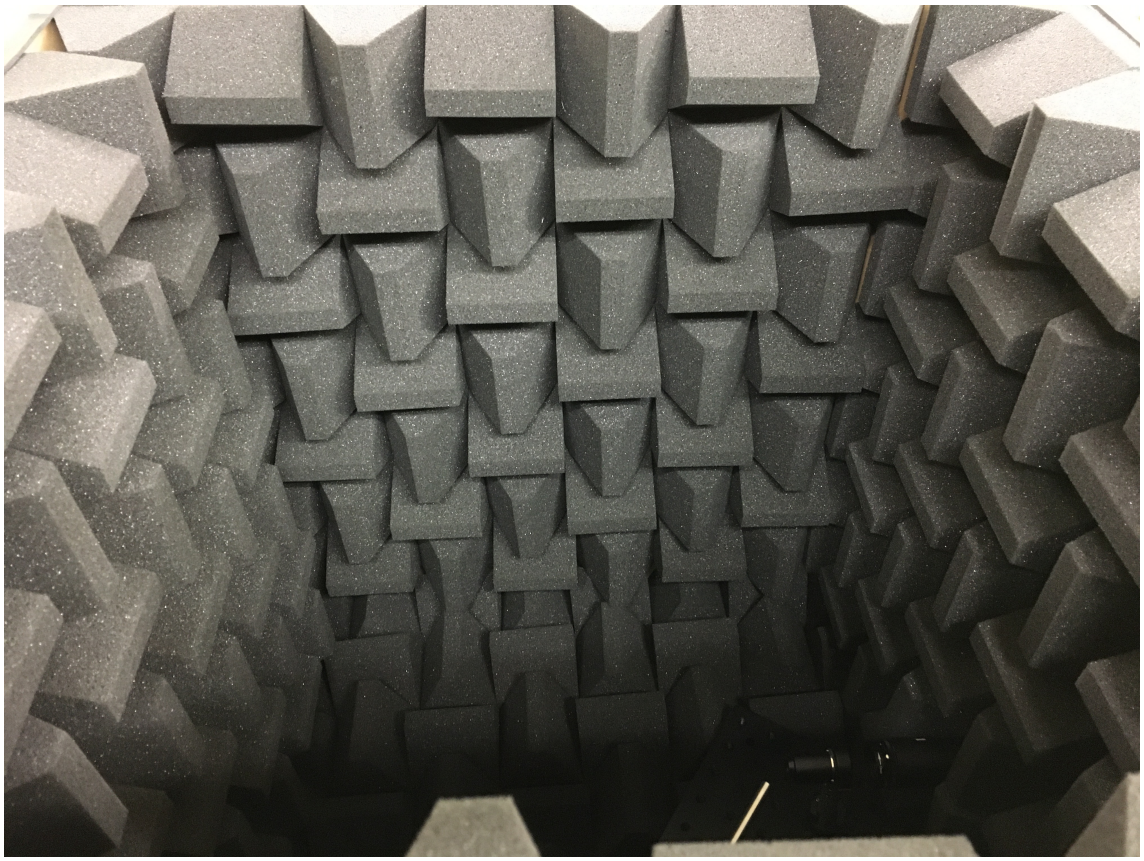

Figure 4.8: Anechoic chamber assembled.

where W is the load (kgf) supported by the vibration insulating rubber, which is calculated by W = mg by mass m and gravity acceleration g. Since the static spring constant of the WF4016 is 40N/mm, the dynamic spring constant is 48N/mm. The performance of vibration isolation is expressed by the index of vibration transfer coefficient τ expressed in[39]

$$\tau = \left| \frac{1}{1 - \frac{f_{vib}}{f_0}^2} \right|, \tag{4.6}$$

where f_{vib} is the frequency of the vibration to be propagated through the vibration insulating rubber. For the $TL_(vib)$ of vibration isolation is calculate as

$$TL_{vib} = 1 - \tau = 1 - \left| \frac{1}{1 - \frac{f_{vib}}{f_0}^2} \right|. \tag{4.7}$$

In the Anechoic chamber section of the experimental results, the calculated results are shown in Fig.5.1.

4.7.3 Transmission losses

Sound transmission loss is an indicator of sound insulation. Sound transmission loss is expressed as the amount of dB value attenuated before and after passing through the shield when the sound propagates through the shield. [40]

$$TL = 10 \log_{10} \frac{I_i}{I_t}. \tag{4.8}$$

where I_i is the intensity (Pa) of sound incident on the shield, and I_t is the intensity (Pa) of sound emitted after passing through the shield. You can see that by expanding the logarithm, the difference in the intensity (dB) of the emitted sound is calculated from the intensity (dB) of the incident sound. In a single wall of airtight homogeneous material, the sound transmission loss follows the mass law theory. A mass law is that when vibration is caused by sound, its vibration velocity is determined by the mass (areal density) of the material. The heavier the mass, the harder the vibration is transmitted, and thus the better the sound insulation. The normal incidence transmission loss TL_N according to the mass law is calculated as

$$TL_N = 10 \log_{10} \left(1 + \frac{2\pi f \rho_s}{2\rho_0 c} \right), \tag{4.9}$$

where ρ_s is the areal density of the shield (kg/m^2), ρ_0 is the density of the air, and c_0 is the speed of sound in the air. Transmission loss considering random incidence is calculated as

$$TL_{random} = TL_N - 10 \log_{10} (0.23 TL_N), \tag{4.10}$$

where TL_random is random incident transmission loss.

Calculate the chamber transmission loss predicted by the mass law based on the data recorded during the experiment. In the Experimental results section, I will conduct anechoic chamber test evaluations and, together with the results, show the mass laws in the experimental parameters in Fig.5.10.

Chapter 5

Experimental result

5.1 Experimental setup

This section describes the measuring equipment used for acoustic measurement.

The audio interface used Roland Corporation's Rubix24[1]. The Rubix24 can record and play back up to 24bit, 192kHz, with an average noise level of-96dBu and a dynamic range of 104dB. The microphone used Earthworks II QTC50[2]. The QTC50 is an omnidirectional microphone with flat frequency response between 3Hz and 50kHz. The speaker is AURA-SOUND NSW2-326-8A[3], using a full-range speaker capable of reproducing sound sources with an accuracy of-10 dB or less between 200kHz and 15kHz. An anechoic chamber was created to measuring the acoustic properties of LIB. Experiments reveal the acoustic characteristics of the chamber.

5.2 Evaluation of anechoic chamber

In order to evaluate the characteristics of the LIB more accurately, I evaluated the acoustic characteristics of the chamber. This makes it possible to measure the acoustic characteristics of the LIB more accurately, since all of the acoustic characteristics of the equipment used to measure the LIB are clarified. Experimental conditions for the simulation are shown in the Table.5.1. The sound velocity c and density ρ_0 of air are calculate as

$$c = \sqrt{\frac{\kappa RT}{M}}, \tag{5.1}$$

and

$$\rho_0 = \frac{1.293P}{1 + \frac{t}{273.15}} \left(1 - \frac{0.378e}{P}\right). \tag{5.2}$$

In the Eq.5.1, where κ is the specific heat ratio (1.403), R is the gas constant (8.314), M is the molecular weight (28.966), and t is the temperature (°C). In the Eq.5.2, where P is the atmospheric pressure (atm), e is the water vapor pressure (atm), and t is the temperature. The water vapor pressure e is obtained by the product of the measured humidity and the saturated water vapor pressure at the measured temperature. Saturated water vapor pressure e_s(atm) is approximated by Tetens equation. [41]

[1]https://www.roland.com/us/products/rubix24/
[2]https://earthworksaudio.com/wp-content/uploads/2018/07/Earthworks-QTC50-Manual.pdf
[3]http://www.ari-co.co.jp/aurasound/NSW2-326-8A/freq.htm

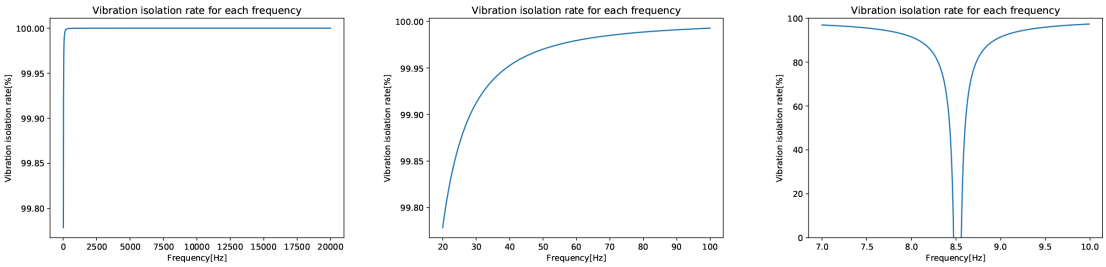

Figure 5.1: Vibration isolation factor at frequencies (a) between 20Hz and 20kHz, (b) between 20Hz and 100Hz, (c) between 7Hz and 10Hz. The vibration isolation factor is 0 or less at the frequency of the natural value.

$$e_s = 0.61078 \exp\left(\frac{17.27t}{t + 237.3}\right). \tag{5.3}$$

Evaluated parameters are vibration isolation in the audible frequency band of the vibration isolation mount used for the installation surface with the ground, acoustic reflection characteristics inside the chamber, and acoustic transmission loss from the outside of the chamber.

5.2.1 Vibration isolation

The weight m of the supported chamber is 16.44kg, and the load W applied to the entire chamber is obtained from the Eq.4.5. Since four WF4016 are attached, the weight supported by one unit is expressed in W/4. The natural frequency of the WF4016 is 8.5Hz, assuming g = 980.7cm/s^2 from the Eq.4.4. The vibration isolation ratio between 20Hz and 20kHz, which are the frequency bands to be actually measured, is shown in Fig.5.1-(a). In particular, the vibration isolation ratio between 20Hz and 100Hz is shown in Fig.5.1-(b), and the vibration isolation ratio between 7Hz and 10Hz across the natural frequency is shown in Fig.5.1-(c).

From these figures, it can be seen that a vibration isolation effect of 99% or more can be expected at frequencies above 20Hz. The center of gravity of the chamber must be at the center of the four isolator because the natural frequencies of the vibration isolating rubber vary with the load. Since the manufactured chamber seals the chamber by closing the lid from the top, the sealing property is improved by placing a weight on the chamber, but care must be taken to keep the center of gravity at the center. The load cause to lower shift the natural frequency, so it does not affect the audible frequency band.

Table 5.1: Experimental condirions.

Temperature	23.4 °C
Humidity	29 %
Atmospheric pressure	1012 hPa
Speed of sound (c)	345.582 m
Air density (ρ)	1.186 kg/m^2
Saturated steam pressure (e_s)	8.346 atm

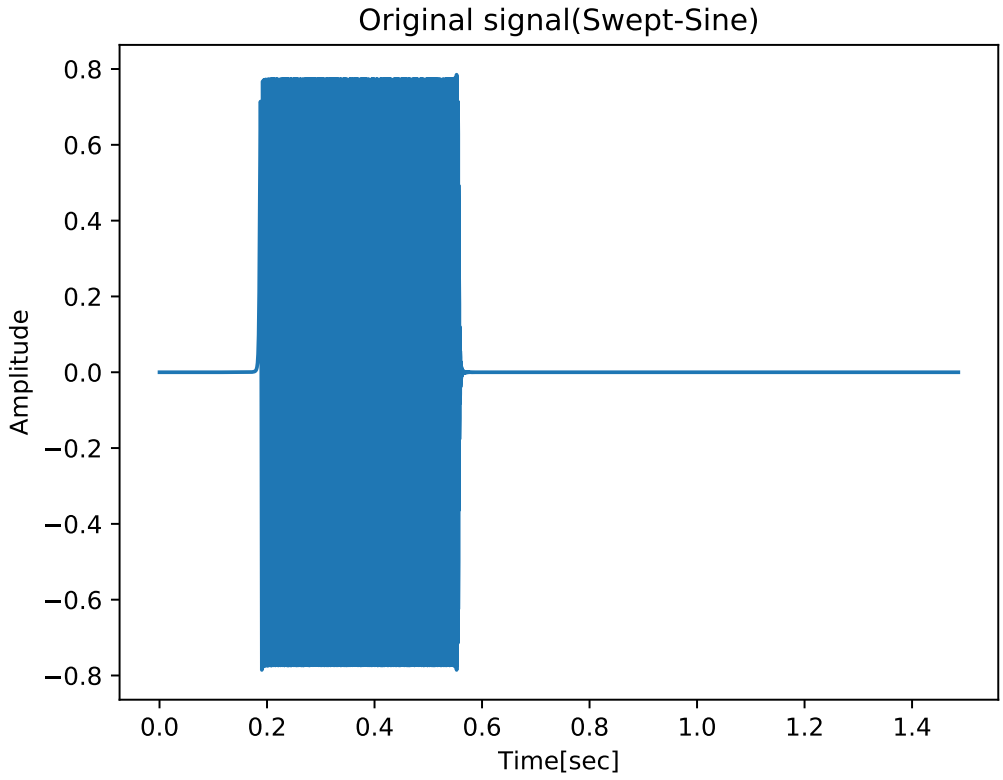

Figure 5.2: Original SS signal. Generated by Python code.

5.2.2 Reflection Characteristic

In order to evaluate the sound absorption performance in the chamber, the reflection characteristics were measured by impulse measurement. Swept-Sine (SS) and Logarithmic Swept-Sine(LogSS) signals were used for the impulse sound source, and the impulse responses were calculated. To increase the SNR, five measurement signals were regenerated continuously, and the response was cut out by the signal length to calculate the summation average. The signal used for the measurement is shown in Fig.5.2, Fig.5.3, and the response measured by the microphone is shown in Fig.5.4, Fig.5.5. The frequency response shown in Fig:5.6 can be obtained by Fourier transforming the response obtained by the measurement and convolving the inverse signal there. Inverse Fourier transform of this gives the impulse response of Fig.5.7 and Fig.5.8.

Since only one peak can be seen in the impulse response, it can be seen that there is no reflection from the wall at all, only the signal arriving directly from the speaker to the microphone is being measured. The reverberation time is 0.05s or less as shown in the Fig.5.7 and the Fig.5.8.

5.2.3 Transmission loss

To prevent measurement errors from occurring due to the directivity of the speakers, the speakers are positioned toward the wall and the microphone receives sound emitted by diffuse reflections from the wall. Connect two microphones to the audio interface and

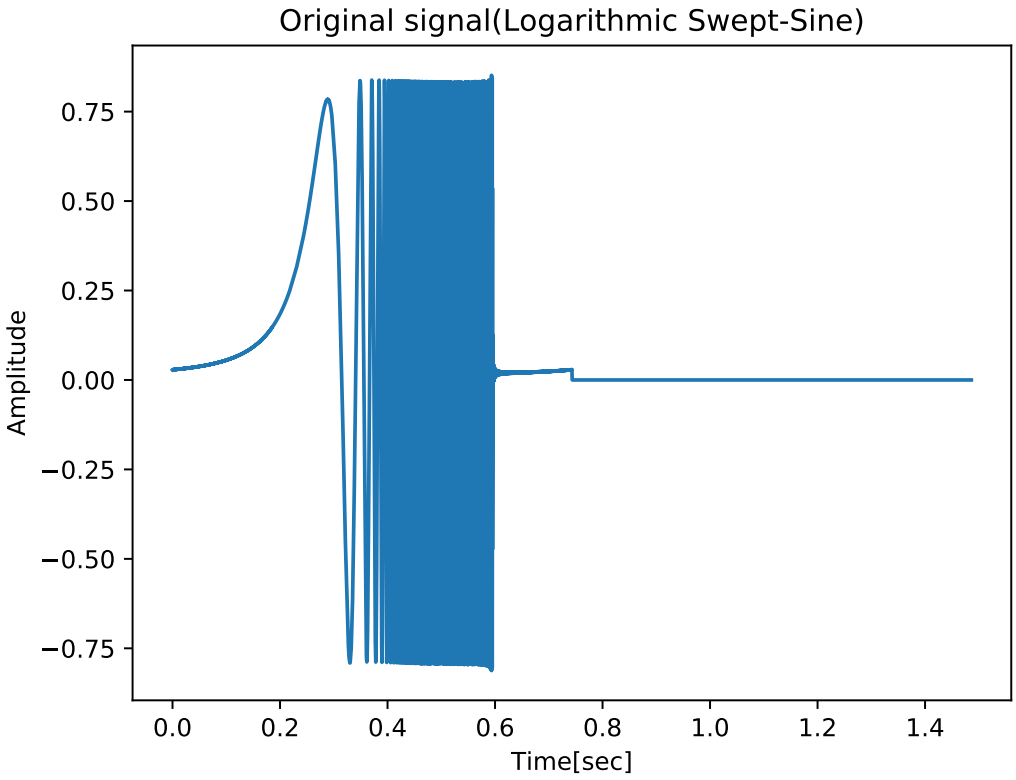

Figure 5.3: Original LogSS signal. Generated by Python code.

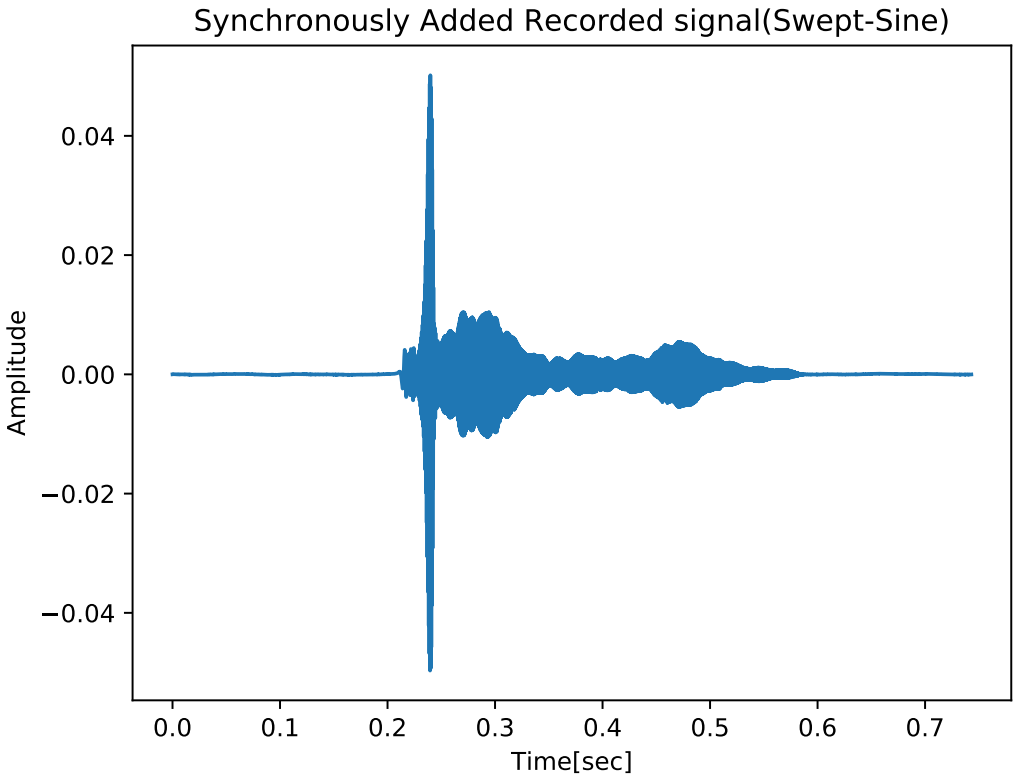

Figure 5.4: Recorded SS signal.

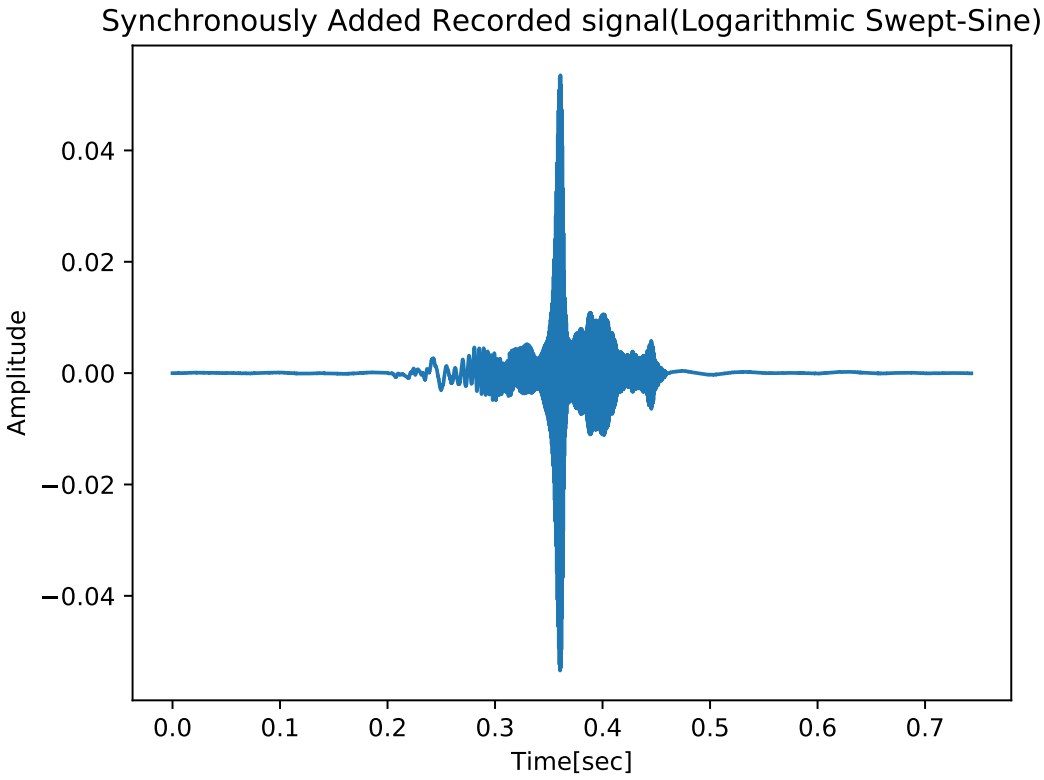

Figure 5.5: Recorded LogSS signal.

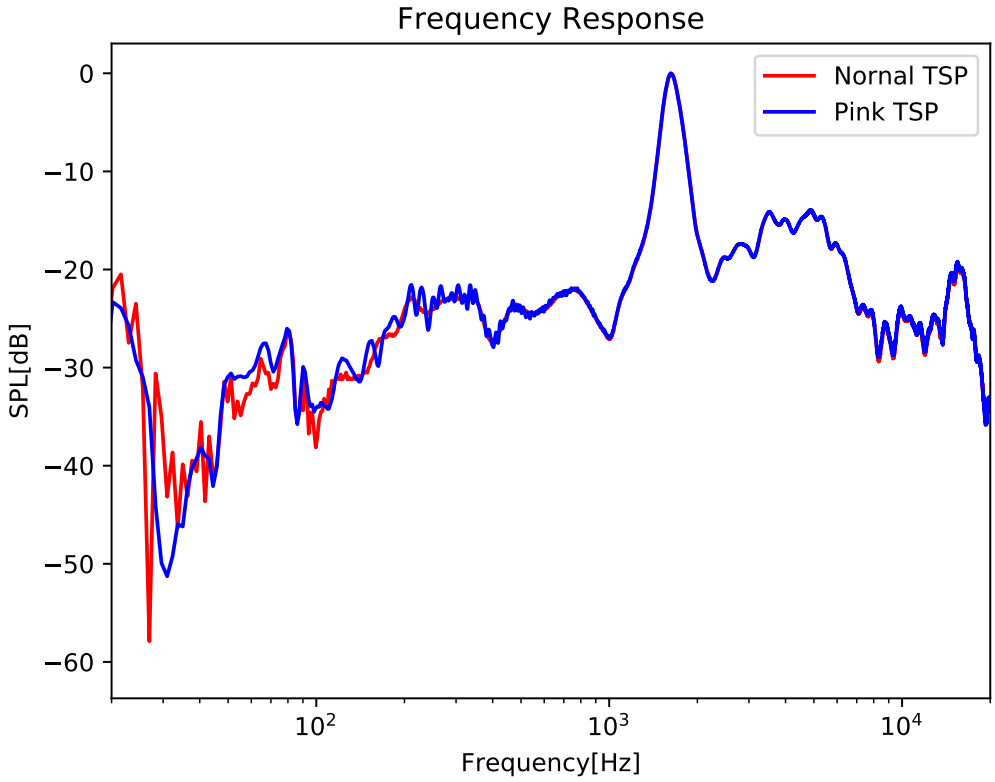

Figure 5.6: Frequency response obtained by convolving the inverse signal.

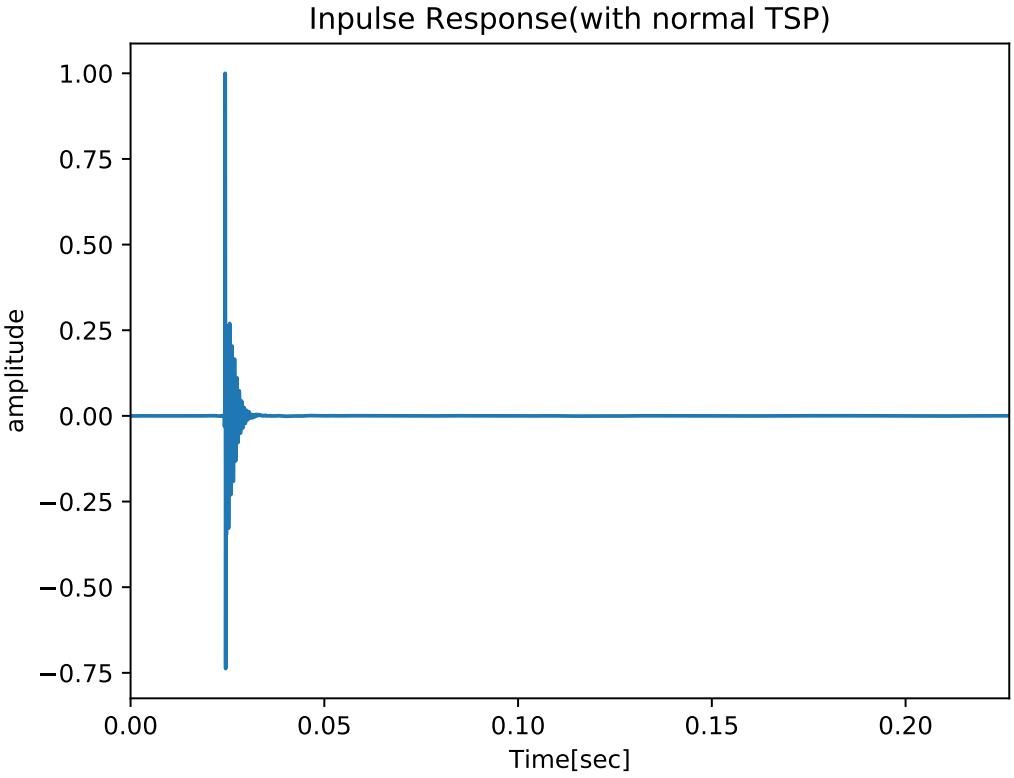

Figure 5.7: Impulse response used SS obtained by inverse Fourier transform of frequency response.

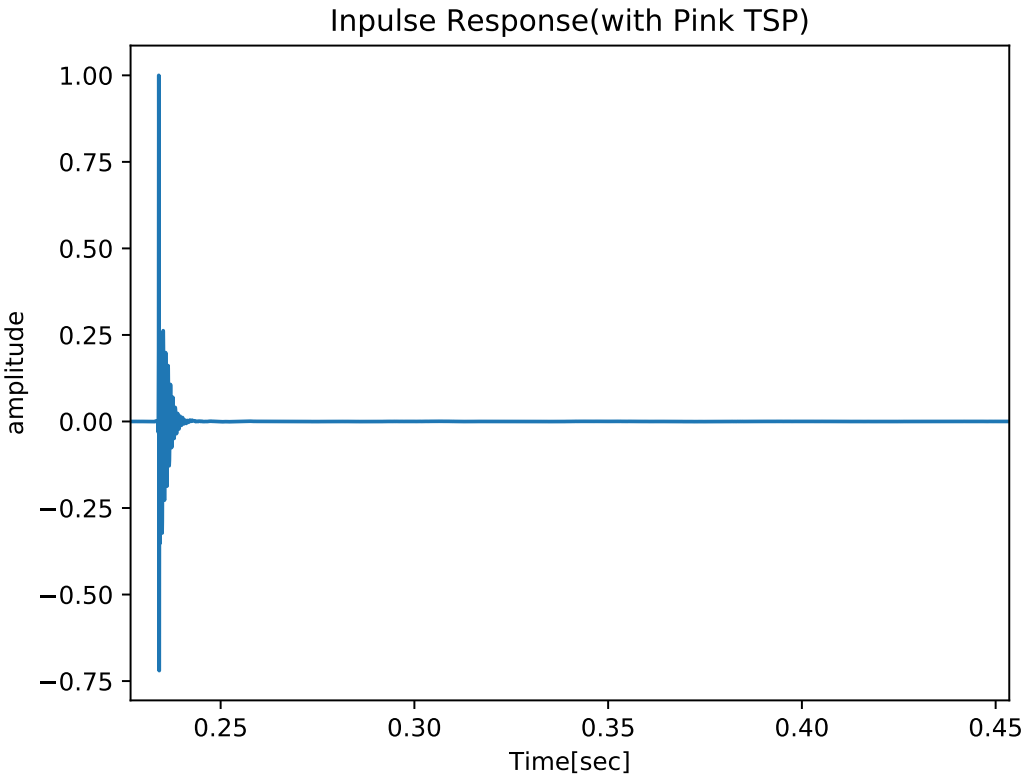

Figure 5.8: Impulse response used LogSS obtained by inverse Fourier transform of frequency response.

install them at two locations inside and outside the chamber as shown in Fig.5.9. Since the microphone is omni-directional, so the microphone was set ignore the direction. RION Co.Lt's pistonphone (NC-72A[4]) is used for unifying microphone input levels. Since the volume inside the microphone was not specified, the correction formula by atmospheric pressure was not used, and the input gain of the audio interface and the recording software was simply adjusted so that the inputs of both microphones are 140dB. From the Table.5.1, saturated water vapor pressure e_s = 8.346, air density ρ = 1.186, and sound velocity c = 345.582. Actual measurement results are indicated by the blue line in Fig.5.10. The transmission loss TL_{random} calculated according to the mass law from Eq.4.10. Therefore, TL_{random} is indicate that the orange line in Fig.5.10.

The measurement results indicate that the transmission loss is increasing along the mass law. The sound pressure level on inside microphone has exceeded the external microphone level in the low range. This is due to the fact that measurements were made assuming transmission loss from one side of the chamber, but actually sound was incident from all sides. At high frequencies, the transmission loss is high and the microphone gain in the chamber is significantly reduced. This makes the SNR worse, causing the measurement results to shake. To improve this, increasing the speaker's sound pressure, also increased the effect of speaker nonlinearity and consequently did not improve SNR.

5.3 Evaluation of LIB sound

In this paper, I propose a method to reproduce arbitrary waveforms with LIB by electronically controlling the shutter of the laser source. I evaluated the characteristics of the sound played by LIB using the created chamber. Laser injection into the chamber was achieved by passing the lens tube through a hole drilled in the chamber wall. Although the laser beam diffuses after it is focused by the lens, the zero-order light propagates in the direction of the laser's travel, creating a risk of igniting the wedge inside the chamber. For this reason, an aluminum plate was inserted by the wall in the beam propagation direction as shown in Fig.5.11.

Objective lenses have a thickness because they consist of multiple lenses. Therefore, the laser should be injected vertically into the center of the lens more accurately. Mounting the objective lens on the lens tube separates the sound from the outside of the chamber, but this makes it difficult to inject the laser perpendicular to the lens. Therefore, a surface plate was placed inside the chamber, and a lens and a microphone were installed there. Since the reproduction of music signals generates LIB for a long period of time, only one chorus was reproduced in consideration of the risk of fire, and an experiment was conducted. If the laser power was too high, the wedges could ignite even with diffuse light. Therefore, I conducted experiments with energy up to 80%.

5.3.1 Frequency characteristics

The sweep signal (Swept-Sine signal) modulated by the PFM method was used to measure the frequency response of the sound played by the LIB. The sampling frequency of the sound source is represented by 496kHz, and the Fast Fourier Transmission (FFT) function of the

[4]https://rion-sv.com/download/manual/NC-72A#NC-72A

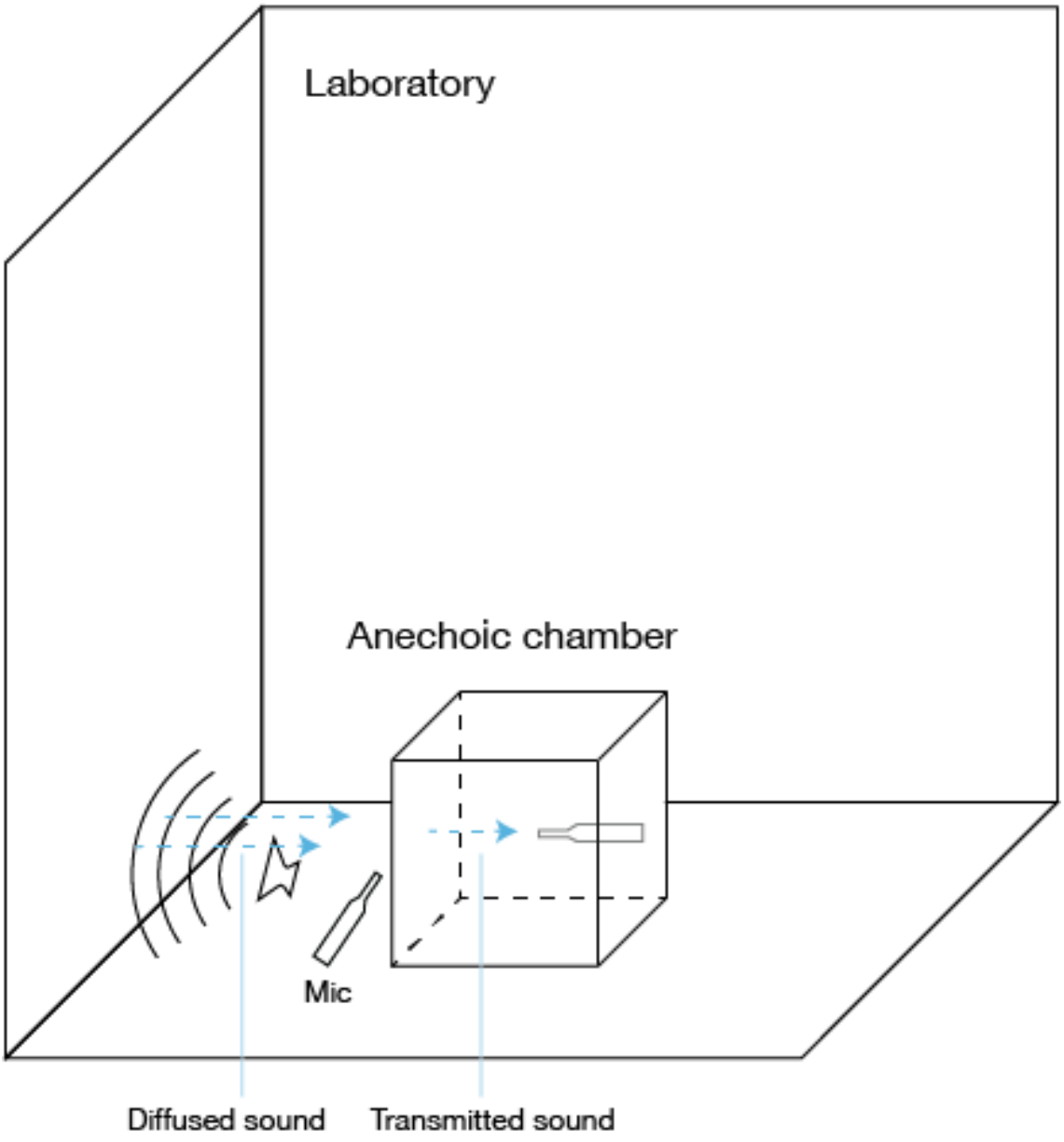

Figure 5.9: Setup for transmission loss measurement. The sound source was aimed at the wall and the diffused sound was set to enter the chamber.

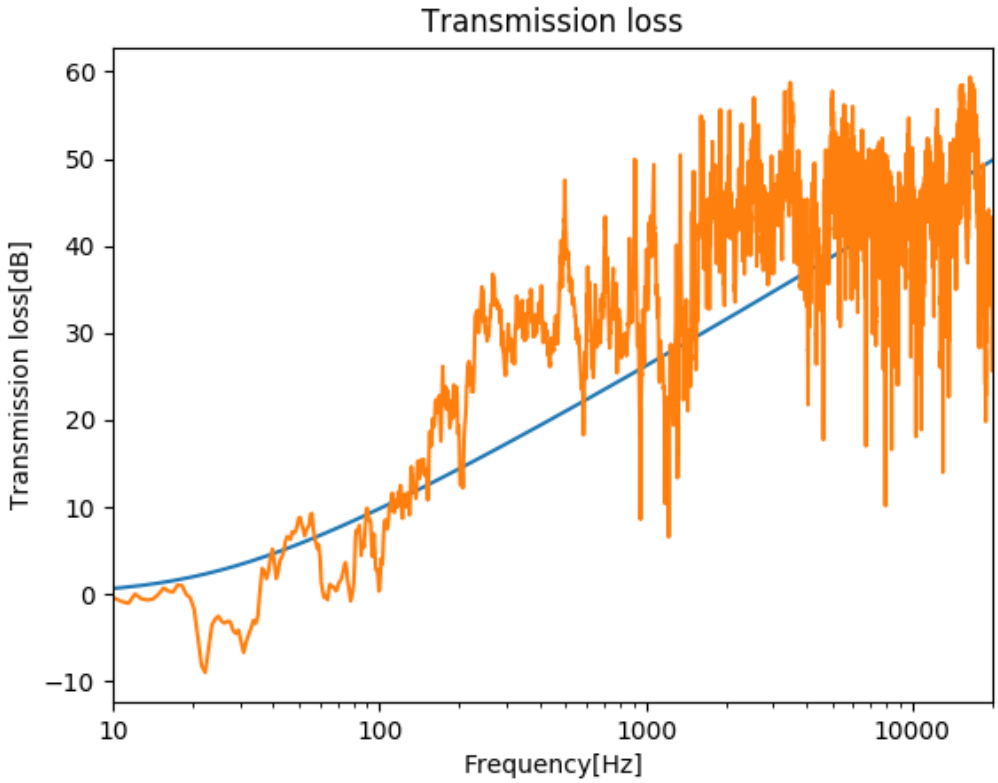

Figure 5.10: The result of measuring the transmission loss of the chamber. Since it is calculated assuming incidence and exit from a single plane, noise is generated, but the value is shifting with a tendency to follow the mass law.

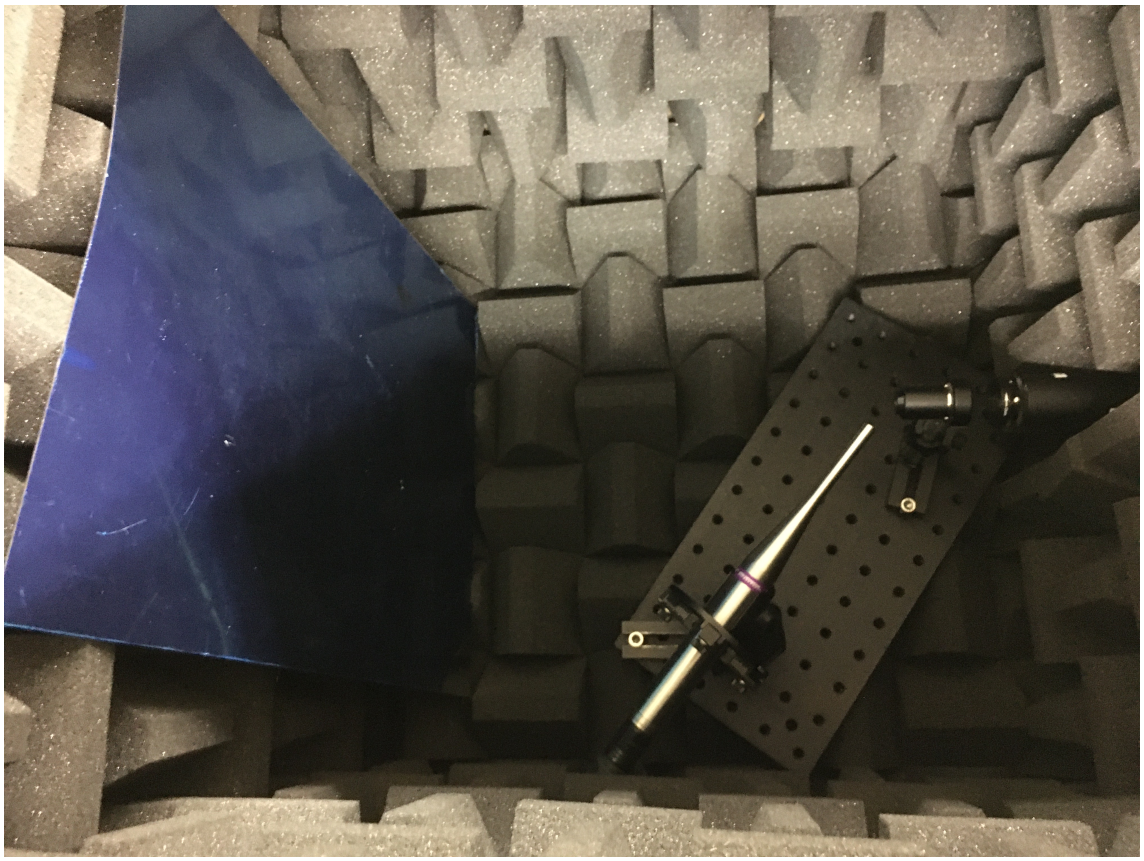

Figure 5.11: Setting for measuring the LIB inside the chamber. In order to prevent ignition, a plate made of aluminum was installed in the traveling direction of the beam.

Adobe Audition was used to analyze the frequency characteristics. I used a Blackman-Harris with a wide dynamic range for the window functions, and chose the largest FFT size (65536).

Background noise is shown in Fig.5.12, frequency characteristics obtained by FFT in Fig.5.13, and spectrogram of the played sweep signal is shown in Fig.5.14. Since there is a background noise peak around 1kHz, he display range of the result is displayed by cutting off the range of frequencies larger than 1kHz. Fig.5.13 indicate that the sound pressure level tends to increase as frequency move to higher one. It was expected to be unsuitable for low-frequency playback because of its small sound source size. There are frequencies with several peaks, but this is noise.

The signal before modulation is a signal that sweeps up to the maximum frequency that can be represented below the sampling frequency. The part where the frequency dropping signal can be seen in Fig.5.14. It is considered to be noise due to the playback of too high frequency components that cannot be acquired by the microphone. The spectrogram of the signal with a sampling frequency of 124kHz Fig.5.15 shows the frequency drop more clearly. When a saw-wave sweep signal is generated by software, the spectrogram actually shows that an integer multiple harmonics of the center wavelength with frequency drops, as shown in Fig.5.16.

Focusing on the area that includes background noise, a peak can be seen around 1kHz. This may be caused by the Helmholtz resonance generated by the lens tube installed to drive the laser into the throat. The Helmholtz resonance calculate as

$$f_h = \frac{c}{2\pi}\sqrt{\frac{s}{Vl}}, \tag{5.4}$$

where V is the volume of the chamber, l is the length of the throat portion (lens tube), s is the cross-sectional area, and c is the speed of sound. The volume of the chamber is 0.36cm^3, the length of the lens tube is 0.18m, the surface area is $0.254m^2$, and the sound velocity c is 345.582m/s from the experimental conditions. From these parameters, the resonance frequency is calculated to be 959.3Hz. The measured value has a peak at 970Hz. The calculated value may have deviated from the measured value due to the influence of the wedges affixed inside or building error.

Between 7k and 8kHz, peaks between 15k and 16k are located at frequencies that are approximately the number of sampling frequencies 496kHz. This is a constant period of noise generated by the DC component added during modulation. Negative values were removed to perform integration when performing PFM. Since the maximum negative amplitude is represented by half the threshold, the noise generated by the DC component is half the sampling frequency. In other words, for a sampling frequency of 496kHz, the center frequency of the noise generated is 248kHz. If the pulses are arranged at intervals of 248kHz, for example, if you take out the value of the pulses one by one, the interval is 124kHz. Similarly, 21.2kHz, 15.2kHz, and 7.6kHz of the audible frequency at the frequency obtained by gradual counting are the frequencies of the peaks that can be checked in Fig.5.13. Now explain this phenomenon mathematically.

The sound generated by LIB arranged in a fixed period T can be regarded as an impulse train. When the impulse signal is modeled as a delta function δ(t) and it is arranged at intervals of period T in the form of a Fourier series, the reproduced signal can be expressed

as

$$h_T(t) = \sum_{n=-\infty}^{\infty} \delta(t - nT), \tag{5.5}$$

where T is the period and t is the time. Since the ideal impulse function contains all frequencies uniformly, its Fourier transform result is 1. Using this property, the complex Fourier coefficient c_n becomes

$$c_n = \frac{1}{T} \int_{-T/2}^{T/2} \delta(t) \exp(-jn\frac{2\pi}{T}t)\mathrm{d}t = \frac{1}{T}. \tag{5.6}$$

Therefore, $h_T(t)$ is

$$h_T(t) = \frac{1}{T} \sum_{n=-\infty}^{\infty} exp(-jn\frac{2\pi}{T}t), \tag{5.7}$$

When this function is Fourier transformed into a function of frequency H(f), it becomes expression

$$H_T(f) = \int_{-\infty}^{\infty} \left(\frac{1}{T} \sum_{n=-\infty}^{\infty} exp(-jn\frac{2\pi}{T}t) \right) \mathrm{d}t = \frac{1}{T} \sum_{n=-\infty}^{\infty} \delta(f - nf), \tag{5.8}$$

and in the frequency domain, it can be seen that it is represented by an impulse train of interval is frequency nf. The Fourier transform of an impulse train results in an equally spaced train of impulses in the frequency domain with a period of 1/T (that is, the repetition frequency of the pulsed laser).

The principle of noise generation focused on the laser's reputation rate is as described above, but in reality, the sound wave generated by the LIB is shaped like a saw wave. When the saw wave is noticed in one period, it can be expressed as a linear function as

$$f_T(t) = -\frac{2a}{T}t, \tag{5.9}$$

where a is amplitude. The Fourier coefficient of a series that repeats this function with a period T is calculate as

$$c_n = \frac{2a}{T^2} \int_{-T/2}^{T/2} t \exp -int2\pi/T \mathrm{d}t, \tag{5.10}$$

using Euler's formula

$$c_n = \frac{2a}{T^2} \int_{-T/2}^{T/2} \left(t\cos(nt\frac{2\pi}{T}) - it\sin(nt\frac{2\pi}{T}) \right) \mathrm{d}t, \tag{5.11}$$

to define $\theta = \frac{n2\pi}{T}t$, Eq.5.11 is

$$c_n = \frac{2a}{T^2} \int_{-n\pi}^{n\pi} \left(\frac{T}{2\pi n}\theta\cos\theta - i\frac{T}{2\pi n}\theta\sin\theta \right) \frac{T}{2\pi n}\mathrm{d}\theta, \tag{5.12}$$

where $\theta\cos\theta$ is odd function and $\theta\sin\theta$ is Even function. Therefore, halving the integration interval in Eq.5.12

$$c_n = \frac{a}{2(\pi n)^2} \int_0^{n\pi} (-2i\theta\sin\theta)\mathrm{d}\theta, = \frac{-ai}{(\pi n)^2} \left[-\theta\cos\theta + \sin\theta \right]_0^{\pi n}, \tag{5.13}$$

from $\sin(n\pi) = 0$, c_n is

$$c_n = \frac{ai}{\pi n}\cos(\pi n), \tag{5.14}$$

When f(t) is expressed in a series using Fourier coefficients c_n with convert $\cos(\pi n)$ to $(-1)^n$ and amplitude a define to 1

$$f_T(t) = i \sum_{n=-\infty}^{\infty} \frac{(-1)^n}{\pi n} \exp(int\frac{2\pi}{T}), \tag{5.15}$$

In the summation formula, the sum when n is positive and when it is negative doubles,

$$i\frac{(-1)^{-n}}{\pi n} \exp(-int\frac{2\pi}{T}) - i\frac{(-1)^n}{\pi n} \exp int\frac{2\pi}{T} = \frac{(-1)^n}{\pi n} 2\sin(nt\frac{2\pi}{T}), \tag{5.16}$$

Therefore, f_T(t) is calculate as

$$f_T(t) = -\frac{2}{\pi} \sum_{n=1}^{\infty} \frac{(-1)^n}{n} \sin(nt\frac{2\pi}{T}). \tag{5.17}$$

As can be seen from 5.17, a saw wave is an infinitely overlapping harmonic with an integer multiple of the center frequency. The result of FFT of the 44.1kHz swept saw wave generated by the Adobe Audition is shown in Fig.5.16. The 21.2kHz noise present in the measured signal is probably due to the nature of such a saw wave. A square wave has a characteristic similar to a saw wave, but it has a characteristic that it contains many harmonics of odd multiples.

Fig5.17 shows a comparison of the frequency characteristics of swept saw waves and square waves. Both waves have frequencies at which harmonics disappear. The difference between saw waves and square waves at this point is significant. In a square wave, the harmonics are swept so that they intersect at the center frequency. On the other hand, a saw wave sweeps so that it intersects at three points: the center frequency, frequency 0, and the sampling frequency. Fig.5.15, you can see how the harmonics disappear even in the measured signal. Since the harmonics sweep toward zero at this frequency, it is clear that the source played by the LIB is similar to a saw wave rather than a square wave.

5.3.2 Effect of sampling frequency

The sampling frequency of the sound source is an important factor in determining the frequency and time domain resolutions of the sound generated by the LIB. At the pulse laser manufacturing, it is difficult to a laser with high repetition frequency and strong peak power. If despite the reptation frequency low, but a sound quality is high, it is indicate that more powerful sound source can be generate. Therefore, I created a sound source file modulated at sampling frequencies of 124kHz, 248kHz, and 496kHz, and acquired the data, respectively. The result of summarizing the three results is shown in Fig5.18.

At 124kHz, noise at 7.6kHz higher than 15.2kHz. However, at 248kHz, their relation reversed. This phenomenon, as can be seen in the Eq.5.17, is presumed to be the result of the increase in the value of 1/T due to the shift of the center wavelength toward the high-frequency side, which further weakens the amplitude of the noise. At 496kHz, noise and signal amplifer differences is smallest than other results. Looking at the whole, it indicate that the SNR is high at high sampling frequencies, but the sound pressure level is falling. This can be attributed to the fact that the frequency divider clock created by the FPGA has a length in the temporal direction, so that multiple pulses are generated when the shutters are opened at one time, causing the energy per pulse output by the FPGA to increase at a low sampling frequency.

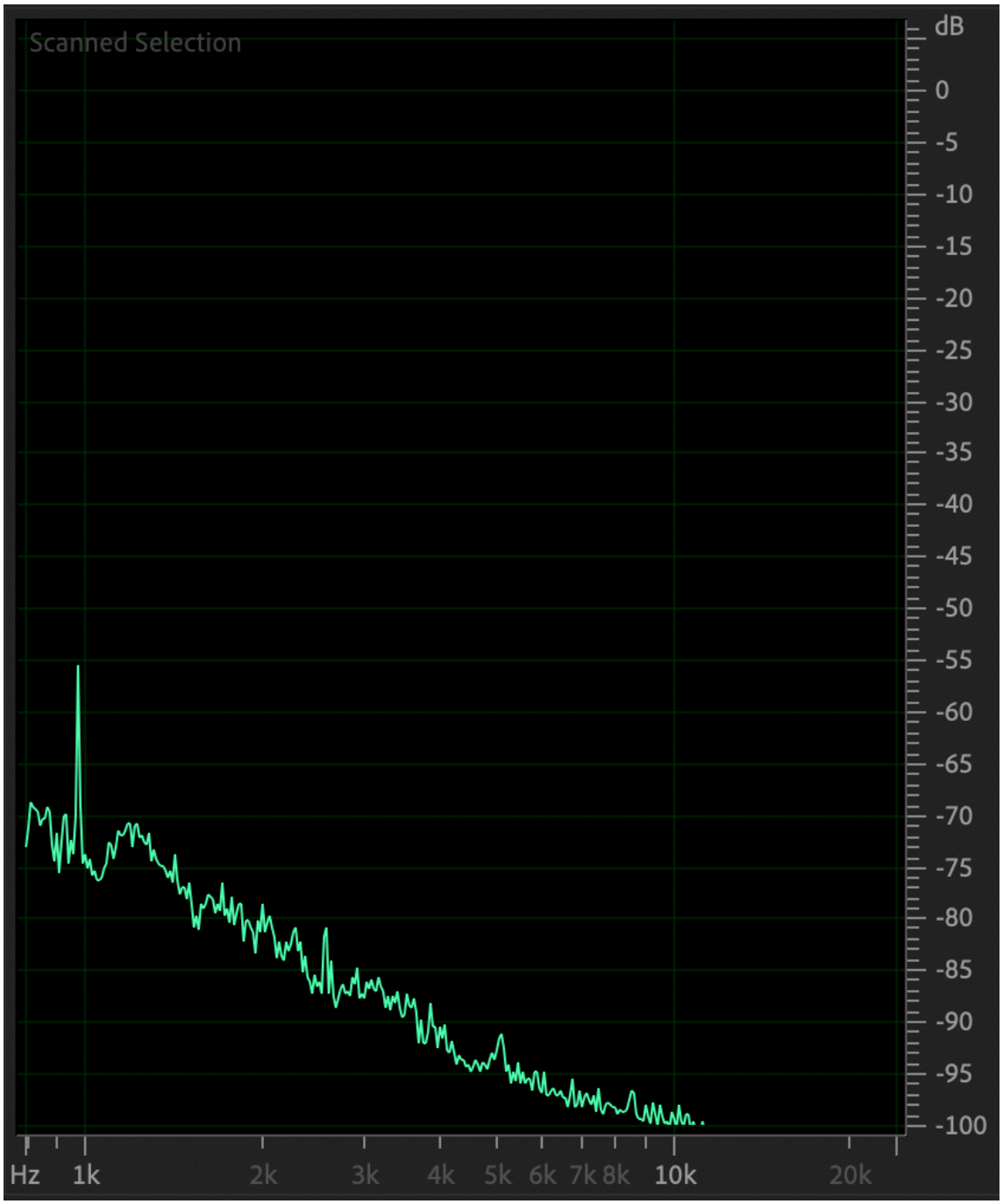

Figure 5.12: Background noise.

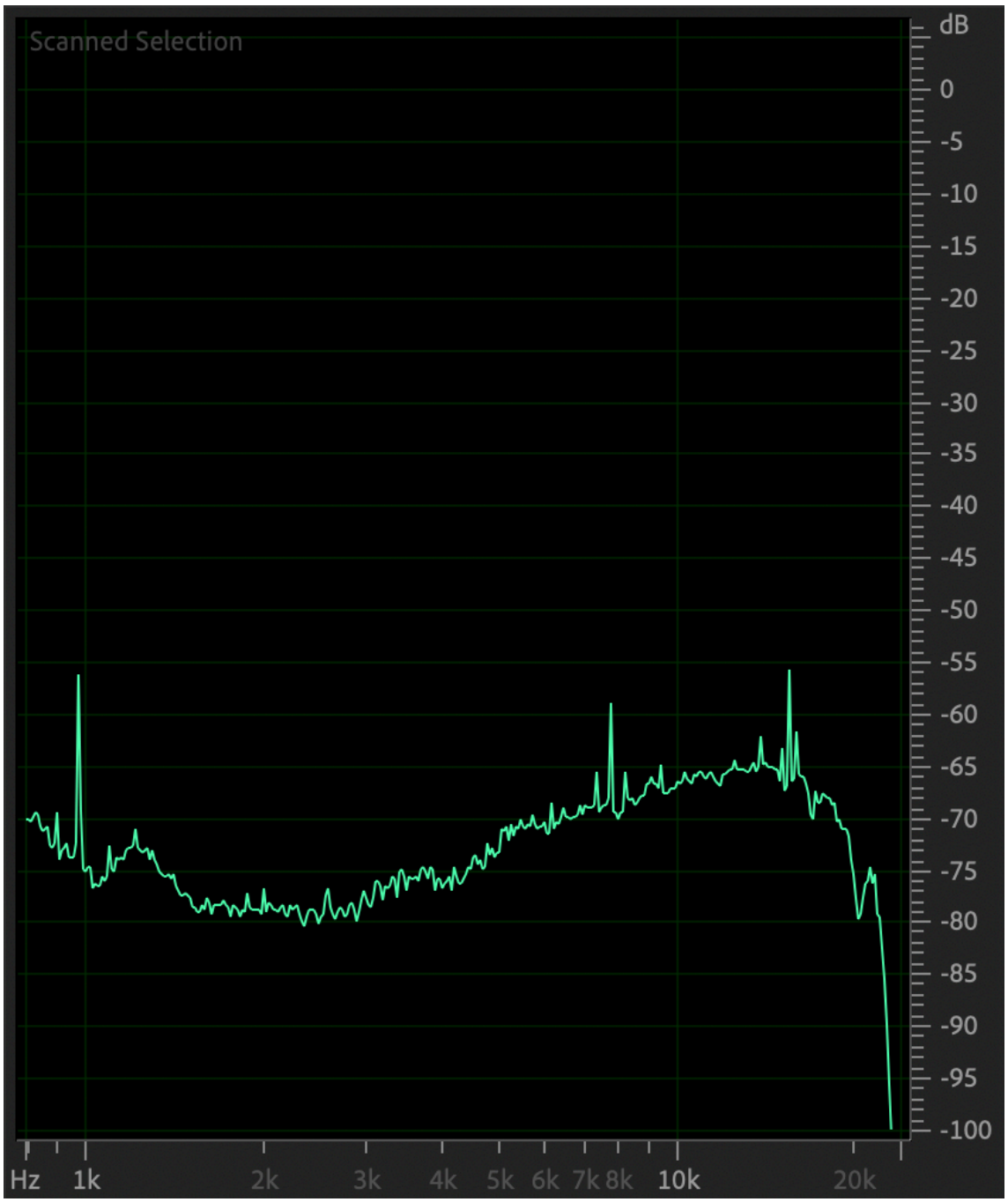

Figure 5.13: Frequency response. The sampling frequency is 496kHz.

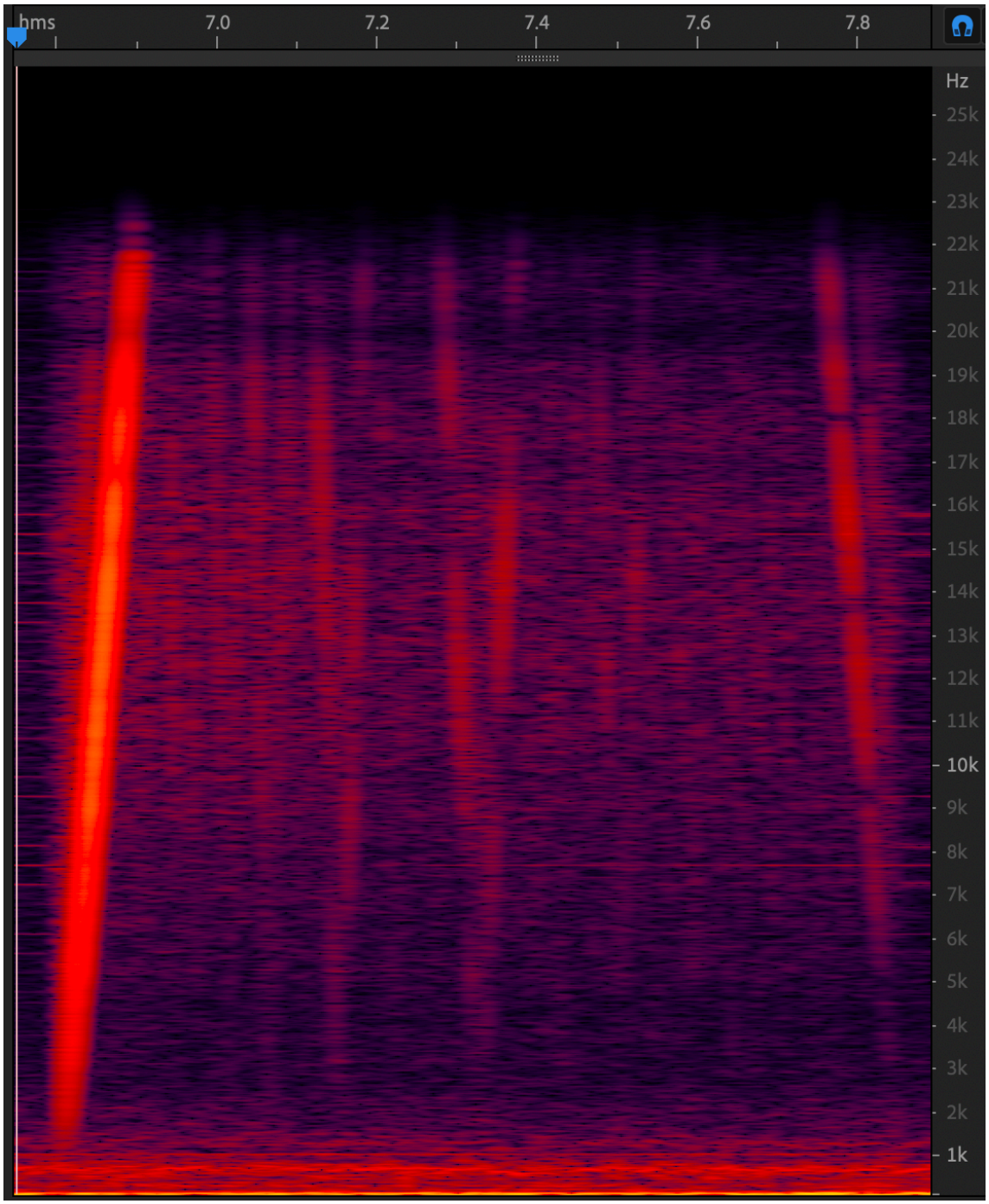

Figure 5.14: Spectrogram. The sampling frequency is 496kHz.

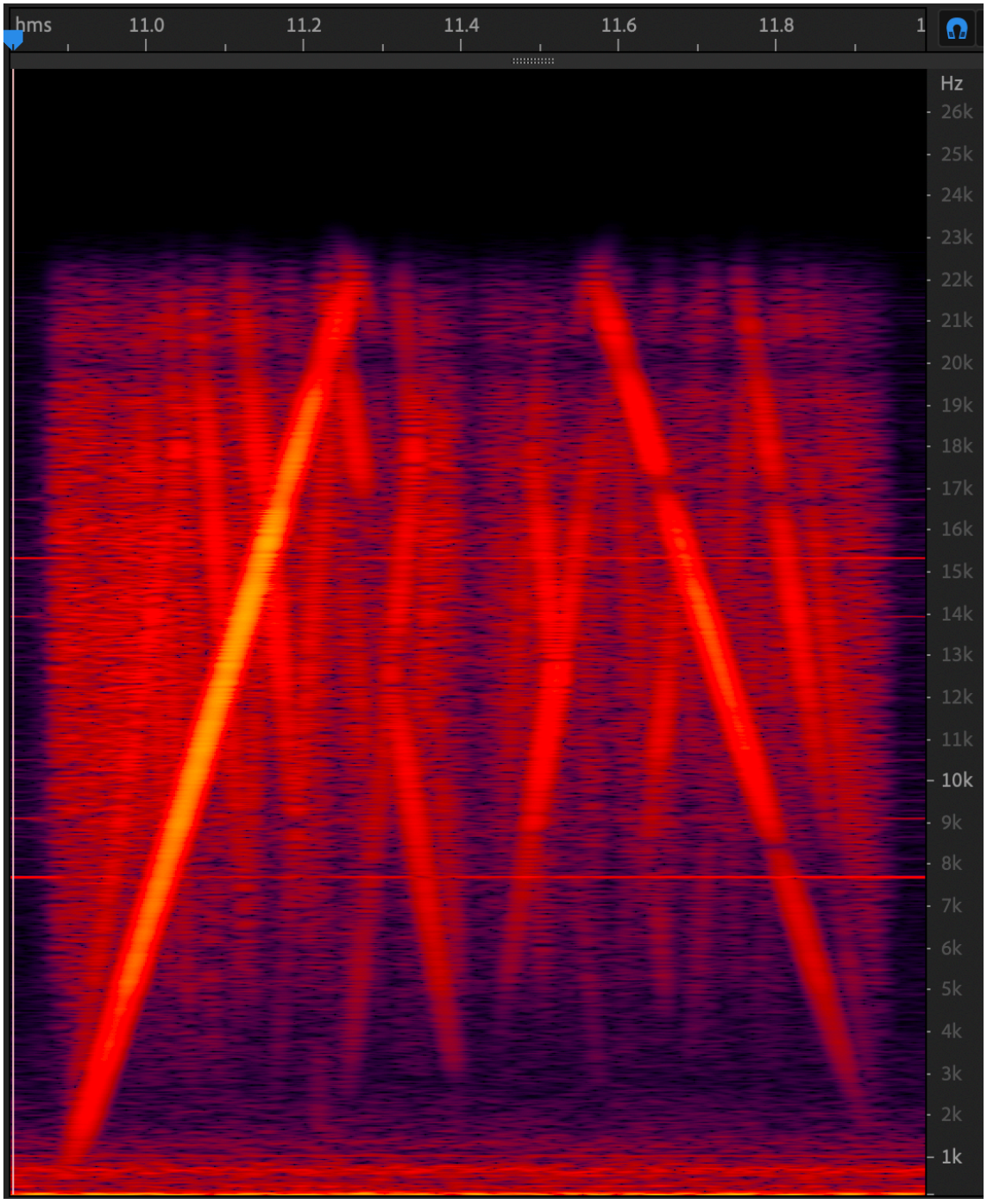

Figure 5.15: Spectrogram. The sampling frequency is 124kHz.

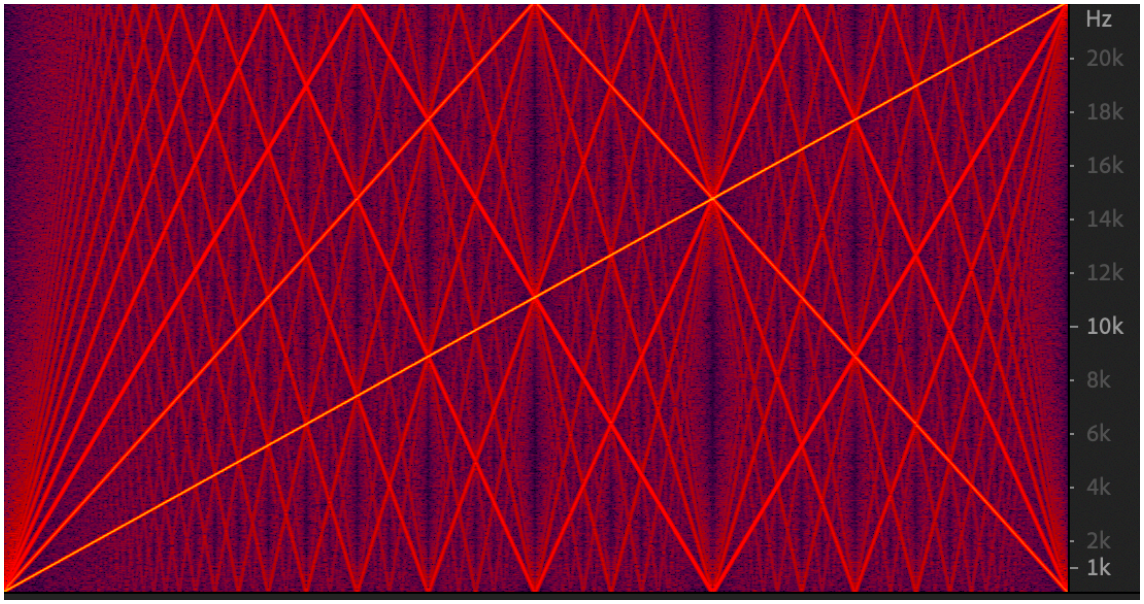

Figure 5.16: Spectrogram of saw wave. The sampling frequency is 496kHz.

5.3.3 Effect of pulse width

Compare the difference pulse width effect. The peak power of the laser pulse is 32μJ at RF Level 80% of 40μJ, and the Spot size of the lens is fixed at 2.5μm, and the pulse width is made to be variable.

I experimented with three pulse widths: 275fs, 550fs, and 1100fs. According to Eq.4.1, the energy density per unit area at each frequency and the sound pressure level at the highest peak (around 15.2kHz) correspond to Table.5.2. The input gain of the measurement system used this time has been raised to a level that is within the limit where the sound generated by the LIB can be recorded without clipping. Therefore, the absolute reference sound pressure is undefined.

In Qin et al., LIB was generated at an energy density of 1.88×10^{11} and $2.83 \times 10^{11} W/cm^2$ by narrowing down a laser with a pulse width of 4 to 6ns, a center wavelength of 1064nm, and a peak power of 800mJ to a diameter of 0.3mm. It has been shown that a sound pressure of up to 181dB is generated with reference to a minimum sound pressure of 20μPa that can be heard in human hearing in this setup. [7]

As can be seen from Table.5.2, the energy density decreases in inverse proportion to the change in pulse width. The FFT results of the actually measured data are shown in Fig.5.19. In this way, the sound pressure level varies depending on the pulse energy, but the relationship is not linear. dB is expressed on a short scale in logarithm to make the sound pressure (Pa) readable. The sound pressure level SPL_{dB} is calculated by the following

Table 5.2: Calculated energy per pulse width and measurement results.

Pulse width (fs)	Energy per unit area (W/cm^3)	FFT Result (dB)
275	5.93×10^{14}	-34.91
550	2.96×10^{14}	-39.33
1100	1.48×10^{14}	-41.65

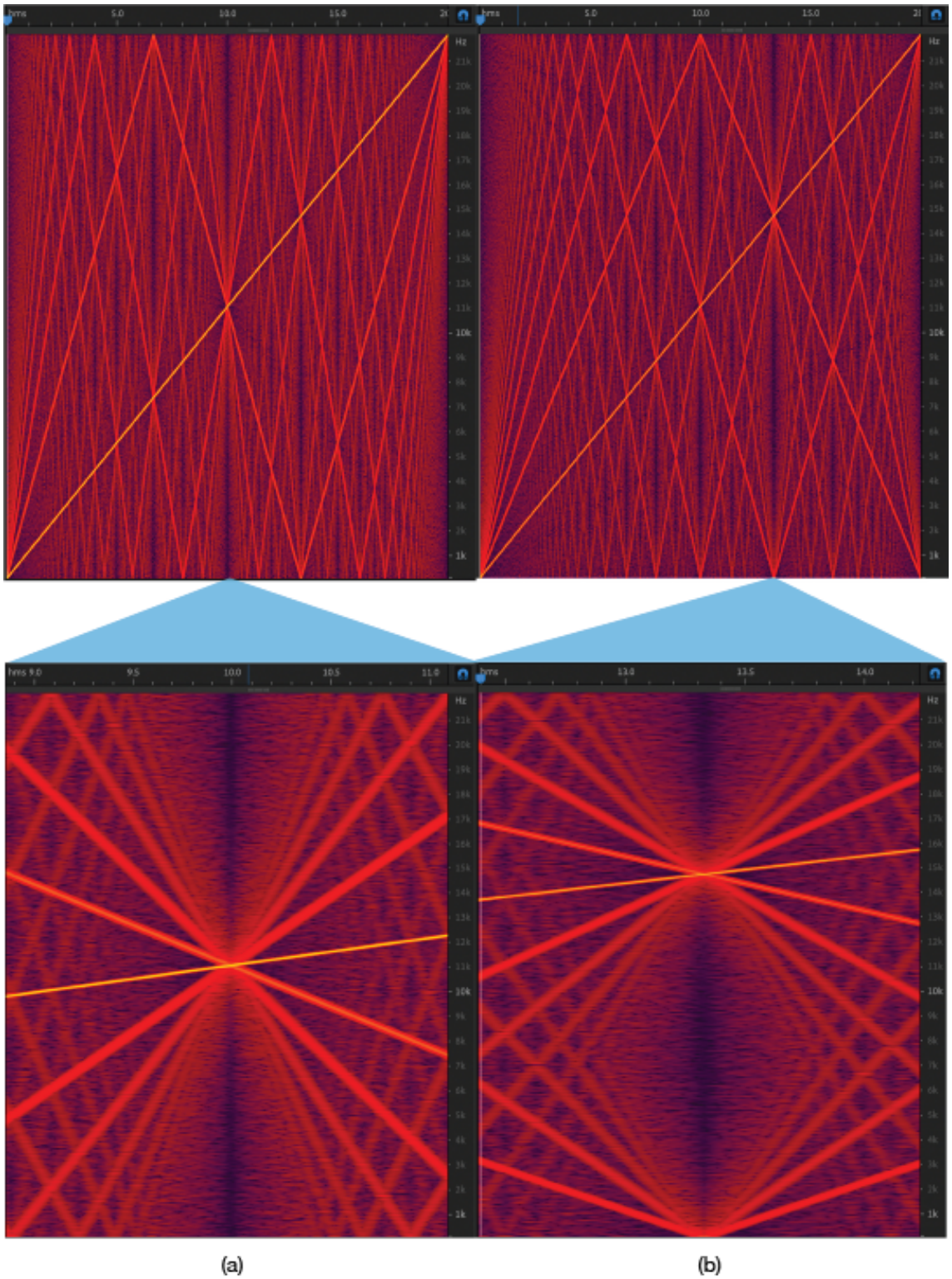

Figure 5.17: Comparison of square wave and saw wave.

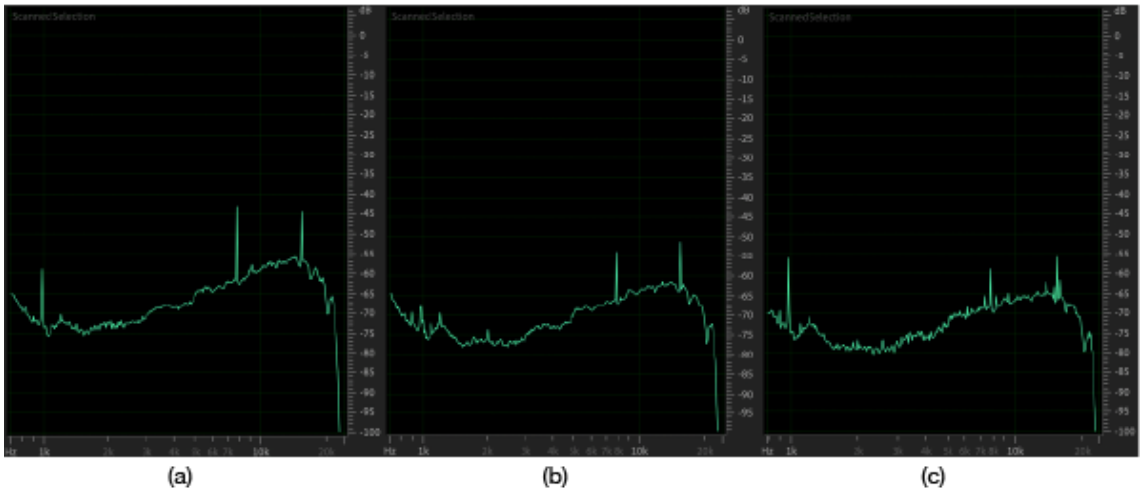

Figure 5.18: Frequency response for each sampling frequency. (a) The sampling frequency is 124 kHz. (b) Sampling frequency 248 kHz. (c) Sampling frequency 496kHz.

formula:

$$SPL_{dB} = 20 \log_{10} \frac{SP_{Pa}}{dB_{ref}}, \tag{5.18}$$

where SP_{Pa} Since dB is a relative measure, the reference sound pressure (dBref) needs to be determined. Since this experiment does not determine an absolute criterion, the criterion is 100, indicating a magnification rather than a Pascal. It is modified from this Eq.5.18, SP_{Pa} is calculate as

$$SP_{Pa} = 20 \log_{10} \frac{SP_{pa}}{dB_{ref}}. \tag{5.19}$$

When the measurement result is expressed by the ratio of power (pulse width) to sound pressure, 4:2:1=2.17:1.30:1. The ratio of sound pressure has some linearity, but it is suggested that the sound pressure may change exponentially as the pulse width becomes shorter. In fact, the sound pressure is $1.30^3 = 2.197$, which is 1.30^{n-1} times greater when the pulse width is n times shorter. This showed that the shorter the pulse width, the higher the energy efficiency.

5.3.4 Accuracy of audio signal playback

The LIB is omnidirectional and can be freely positioned in the air. In the field of stereoscopic sound, the most common method is to use multiple speakers to control the phase difference to illuminate the position of the sound source. If this method can be applied, the sound field can be more freely reproduced and a three-dimensional sound field can be reproduced. Therefore, I performed audio signal playback and signal comparison before modulation. Since LIB must be generated for a long time for audio signal playback, recording is stopped with a one-chorus for safety reasons. The spectrogram of two types of sound source data is shown in Fig.5.20. The original signal is arranged in the upper row of the signal that was played back in the lower row. When the waveforms are actually arranged, the main signals below 1kHz are hidden by the background noise, but it can be seen that they can be reproduced faithfully even when compared with the spectrum of the original signal. As verified in the Frequency Response section, when playing back at low frequencies, the sound

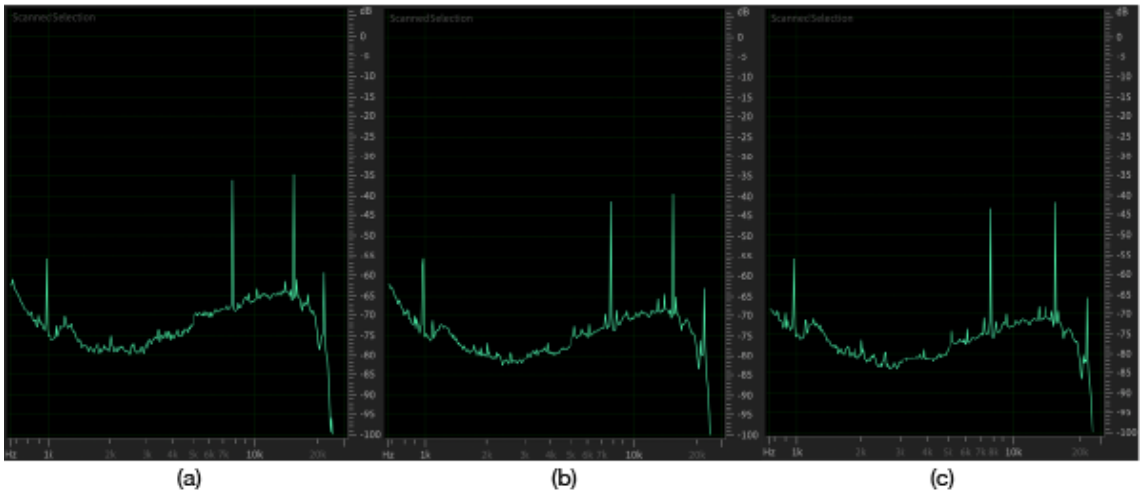

Figure 5.19: Frequency response for each pulse width. (a) Pulse width 275 fs. (b) Pulse width 550 fs. (c) Pulse width 1100 fs.

pressure level is low and the waveform cannot be reproduced at frequencies below 1kHz. AudioA used in the various effected electric sound beeing classified UK Rock, Audio B only used acoustic instruments. When you actually hear it, you will hear the sound sticking to your ears due to the harmonic content, so in order to use it in audio playback, more cleary modulation method is required. In addition, in a AudioB where there are many conditions close to silence, noise at certain frequencies is particularly noticeable. Harmonic distortion allows you to check noise with similar frequency characteristics around a noise with a constant frequency. Masking areas close to the absence of a signal with noise may cause the noise signal to rise randomly and mask a sound with a constant frequency.

5.3.5 Noise reduction by modulation

Since it was determined that the source of the noise at a certain frequency was modulation. Some challenge was experimented with several filtering processes to eliminate the noise after modulation.

Because a DC component with half the amplitude of the maximum amplitude was added during modulation, the integration process resulted in a pulse at a frequency 1/2 of the sampling frequency in the case of silence. When I tried to cut off the odd-numbered pulses and treat the sampling frequency as half, the noise was removed in the first silent part, but after the signal was played, the timing at which the noise was generated changed, and the resulting noise could not be removed. Therefore, I checked the signal back from the timing where hi was output after modulation, and if hi was generated by one flying, I performed the processing of setting the signal to 0. For a sweep signal with a sampling frequency of 496kHz, when hi is one piece and 500 pieces are continuously skipped, it is regarded as noise, and the frequency characteristics and spectrogram of the signal after removing it are shown in Fig.5.21. The frequency characteristics measured by cutting off only the playback part of the sweep signal are shown in Fig.5.22. The first noise has been cleared, but the noise after signal playback has not been cut off, and you can read how 248kHz noise is generated intermittently. If you look only at the part where the sweep signal is playing, you will find

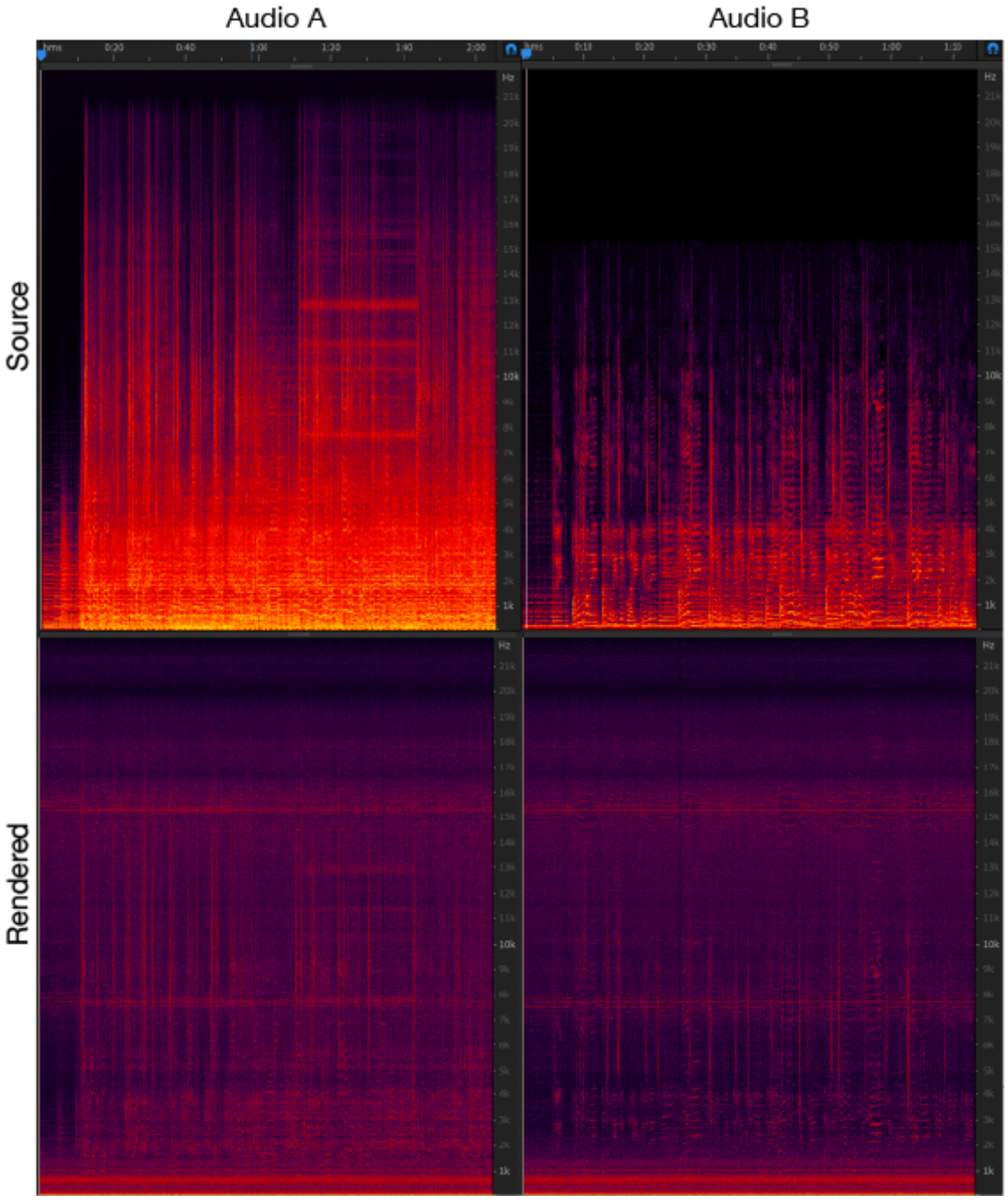

Figure 5.20: Comparison of the source audio file (upper row) and the rendered sound (lower row).

that it has almost the same characteristics as the signal before filtering. It is probable that the noise generated in the silent part after the signal can be eliminated by filtering from the opposite direction as well.

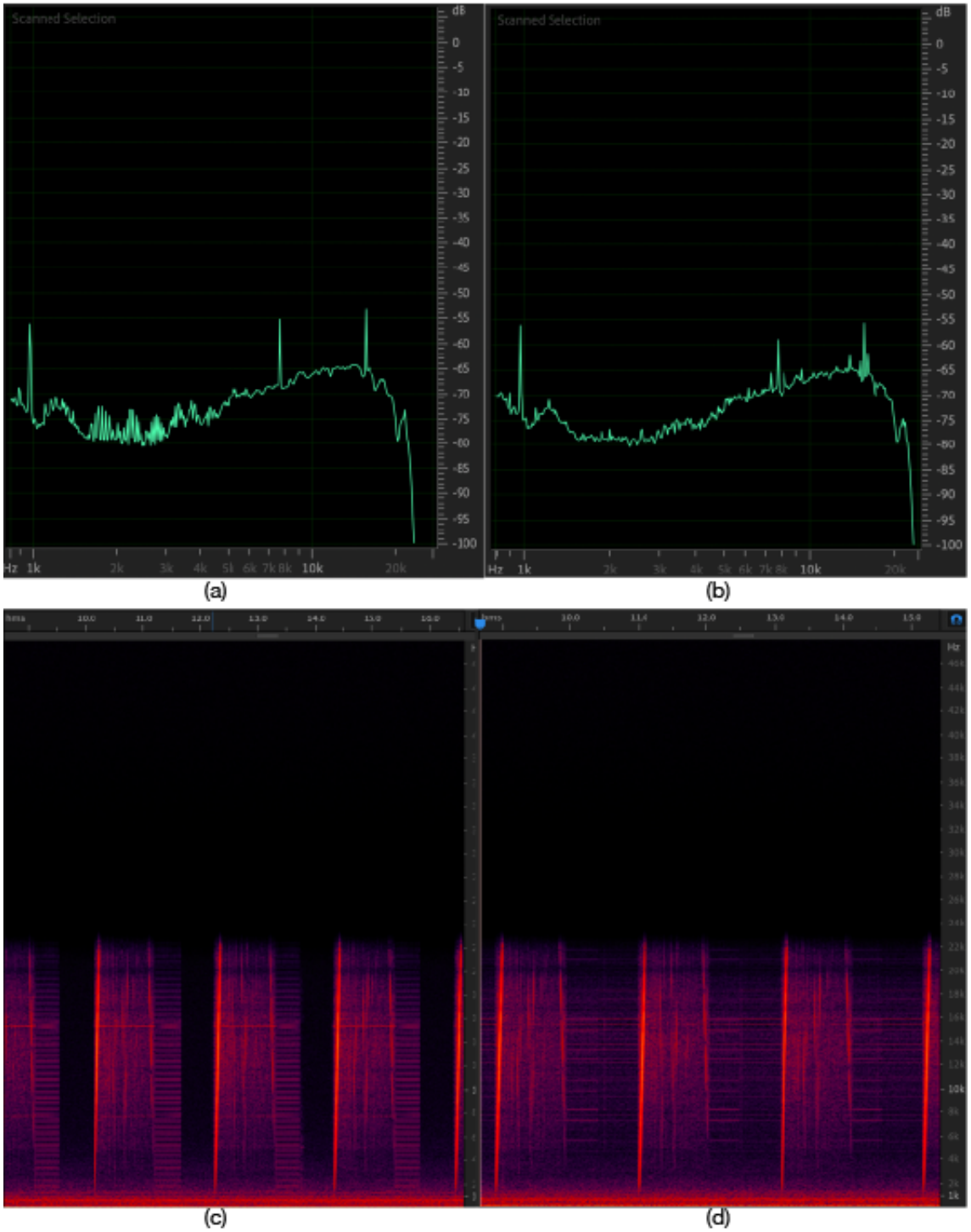

Figure 5.21: Comparison of the signal after noise removal and the signal without noise removal. Frequency spectrum (a) Signal with noise removed, (b) Signal without noise removed. Spectrogram (c) Signal from which noise has been removed, (d) Signal without noise removal.

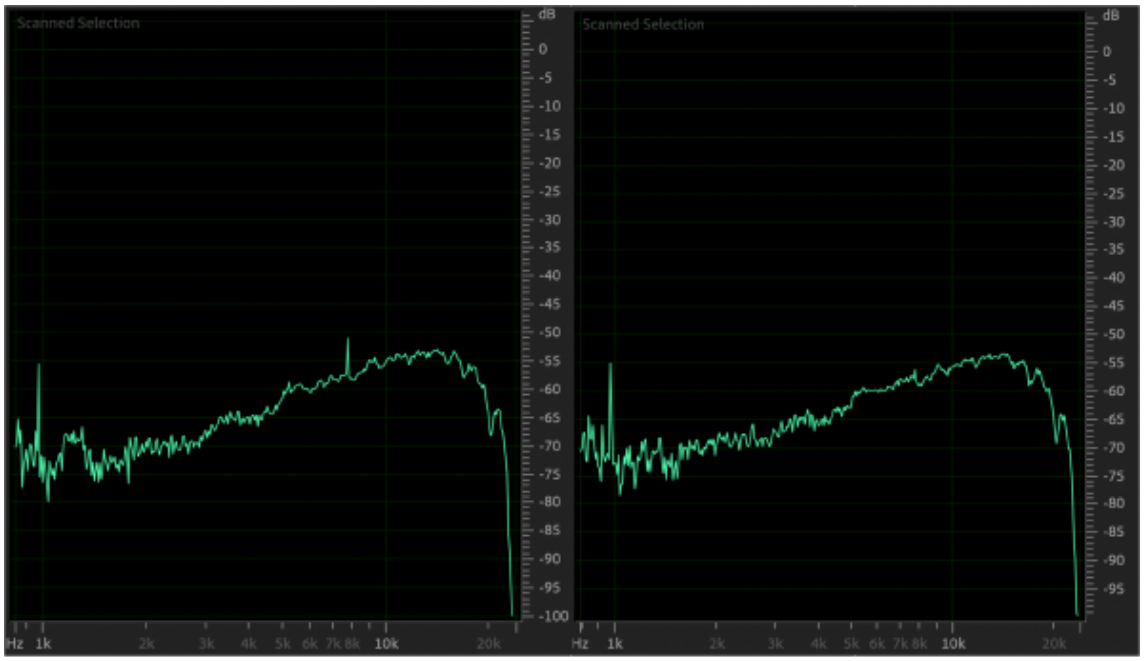

(a) (b)

Figure 5.22: Frequency spectrum when one signal is cut out with playback time up to 20kHz. (a) Signal from which noise has been removed. (b) Signal without noise removal

Chapter 6

Applications

6.1 Acoustic measurement using a reduced model

In acoustic measurement, the frequency and phase characteristics of the system (room or acoustic equipment) can be measured by measuring the impulse response. LIB are high repeatability and have attracted attention as an impulsive sound source for use in room acoustics, [42], which can potentially meet the omnidirectional requirements stipulated in International Organization for Standardization (ISO) 3382-1. In reality, however, the impulse response can only measure the linear characteristics of the system. Nonlinear phenomena include various distortions such as harmonic distortion and crowded modulation distortion, hum noise, internal noise of measuring equipment, and other external noise. In order to take these into account, the signal used for the measurement must be designed. Noise can be eliminated to some extent by adding and averaging (synchronous addition) something like white noise. With short-duration pulsed waves, the frequency-by-frequency power is low, and in addition to the system's transfer functions, the system is unable to obtain enough signal noise ratio in the frequency band, making the number of synchronous additions unrealistic. Therefore, the methods of measuring signals such as Maximum Length Sequance (MLS) [10] and Swept-Sine signal [11, 12] and calculating the impulse responses are now the mainstream. MLS is a periodic pseudo-random signal with almost the same stochastic characteristics as white noise, and Swept-Sine signal is a time-expanded signal whose phase of the impulse signal is proportional to the square of the frequency. MLS and Swept-Sine signal provide close measurements, but there are slight differences in characteristics. In MLS, the effect of harmonic distortion called "distortion peak" is likely to occur. Increasing the power in order to obtain SNR in the low frequency band results in a reverse decrease in SNR at high frequencies [43]. On the other hand, MLS is more suitable for measuring impulse responses with faster calculation speed and longer calculation time. The Swept-Sine signal is highly scalable and has derived signals such as [43] and [44, 45] in the Logarithmic Swept-Sine(Log-SS) of a longer low-frequency regeneration time to obtain SNR in the low-frequency range, and a constant signal-to-noise ratio Swept-Sine (CSN-SS) designed to keep SNR constant in the full-frequency range. To reproduce a signal suitable for acoustic measurement such as these, a means of reproducing an arbitrary waveform is required. If I apply the sound source reproduction method proposed in this study to experiments of room acoustic measurements using LIB, which has been verified using only simple impulse signals, I can expect further improvements in SNR. In addition, it is anticipated

that the indoor acoustic measurement test with a reduced model using electrode plasma will enable more accurate measurement by taking advantage of the stability of the LIB and the superiority of not generating reflected sounds from the sound source. The impact of LIB nonlinearity on the measurement should be thoroughly verified.

6.2 Free positioning airborne speaker

Since the laser used in this study lacks peak power, there are restrictions on the volume and focal length of the lens to be condensed, and the function as a speaker is still insufficient. Recent studies, however, have also developed an atomic-second (10^{-18} s) pulsed laser with instantaneous power up to 2.6GW [46] and a PW-order famtosecond laser [47]. The development of higher-intensity lasers allows for longer focal lengths of lenses used for condensing and higher volume. Thus, it is expected that the application as a speaker with higher degree of freedom of spatial arrangement becomes possible. The potential applications of this feature improvement are:

1. It can be arranged like a planar sound source by simultaneously generating a plurality of points of LIB.
2. Object-based stereoscopic sound can be produced by designing the movement of the sound source.
3. It can be applied to acoustic measurements in larger spaces.

6.2.0.1 Improvement of volume and frequency characteristics

LIB is only a few micrometers in diameter, so it is not suitable for bass playback or high volume playback. However, by arranging the LIB at multiple points, it can be regarded as an approximate larger-sized sound source, so that it is possible to improve the frequency response and play back loud sounds. As for the volume level, there is a possibility that it will not be improved because the energy of each LIB decreases. However, when the sound source is arranged in a plane, the elements propagating in a plane perpendicular to the plane formed by the point cloud of the LIB become stronger, and as a result, the sound can be heard at a high volume level.[36]

6.2.0.2 Application to 3D sound

In stereoscopic sound, a mechanism is used by humans to estimate the position of the sound source so that the sound source is perceived as if it originated from anywhere other than the speaker. Phase difference and volume difference interaural level difference (ILD) of sound heard from both ears And interaural time difference (ITD) is used to determine the sound source orientation. This can be used to deliberately create a phase difference to create the illusion of a sound consisting of some direction. There are many ways to achieve stereoscopic sound. For example, there are binaural recordings that faithfully measure ITD and ILD by using a dummy head to record sound at the position of the human eardrum, and multi-channel audio systems that place five speakers and one woofer around the listener to reproduce the sound field.[48] Binocular recording can be easily performed by using an earphone-type microphone called a binaural microphone. It is also popular and popular

because only the earphones are necessary for playback. However, in general, the sound field that can be reproduced with stereoscopic sound is limited to the area within the space surrounded by the reproduction equipment, so a multichannel audio system like a 5.1ch speaker is required to dynamically express a wider sound field. In multi-channel audio, the number of channels corresponds to the number of speakers, and the more channels, the more faithful the sound field can be reproduced. Since it is difficult to express the sound field in the vertical direction with speakers arranged flat against the head, there are also studies in which speakers are arranged in a three-dimensional manner using a huge system that uses the entire room, such as 22.2ch.[49] The system proposed in this paper uses a LIB that can be freely positioned in space, so that a more realistic sound field can be reproduced with a simple configuration. However, there are restrictions on the number and volume of sound sources that can be played simultaneously, and the current price of lasers does not make it realistic for households to introduce this technology. I expect the development and diffusion of laser technology. The high power lasers required for the generation of LIB are hazardous classified as Class 4 in accordance with International Electrotechnical Commission 60825-1:2014 and should be used with extreme caution when applying them as loudspeakers.

6.2.0.3 Application to acoustic measurement assuming directional loudspeaker

In indoor acoustic measurements using the current scale model, only the case where a sound source spreading in a three-dimensional direction is assumed is considered. However, directional speakers utilizing ultrasonic technology are practically used and are likely to be incorporated into future stereoscopic sound systems. The size of the sound field felt by stereophonic sound is limited to the size of the space surrounded by the speakers. Therefore, a huge system with 24 speakers arranged in every corner of the room has been devised to provide a wider sound field [49]. However, ultrasonic speakers allow a wall to diffuse an ultrasonic beam so that it sounds as if it were coming from that point, providing a wider sound field than placing a large volume of speakers [50]. It is difficult to prepare a micro sound source with directivity in the conventional method. Using the technique described in this paper, which generates sound using lasers, multiple-point LIB can be generated freely by using microlens arrays for condensing lenses or by controlling wavefronts using Spatial Light Modulator (SLMs). It has the potential to be applied to the simulation of an ultrasonic beam with directivity by generating multiple-point LIB inside a reduced model, giving directivity to specific frequencies. Experiments have revealed that the directivity can be controlled by arranging laser pulses in an array. [36]. Therefore, it is anticipated that the sound generated by the LIB contains many harmonics, and therefore, it is possible to make a control that strongly radiates any frequency in a specific direction depending on the distance of the multi-point arrangement. Previous studies have mentioned that increasing laser pulse energy increases the sound pressure of point sources produced by LIB, but reduces repeatability and reveals variability [6]. It is expected that the sound source generated by the LIB is affected by the shape of the plasma tail formed by the filamentation so that the directivity of the sound source due to electric discharge varies with the distance between the electrodes. It is necessary to clarify the relationship between repeatability and laser pulse energy of sound pressure in order to use it as a sound source for measurement. In addition, since the frequency characteristics of the LIB depend on the high frequency range,

the sound pressure level in the low frequency range does not reach the sound pressure level required for sound measurement. When measuring within a reduced model, there is no problem because playback of the low range is not required.

6.3 Combination with aerial image

Ochiai has drawn an aerial image by scanning the focus to generate LIB [5]. By combining the methods proposed in this study, sound can be generated from the aerial image itself. LIB occurring in the air are aesthetic, and the aerial image drawn thereby enables artistic representation. In addition, the possibility of expression is greatly expanded by designing and playing any sound. Therefore, pulsed lasers can be expected to be applied to art, such as incorporating them as part of a video product or creating aerial images that combine multiple LIB. Problems with this application are discussed in the discussion section.

Chapter 7

Disucussion

7.1 Effect of LIB harmonics

In the sound source reproduction of LIB, the harmonics are generated by the nonlinearity of the sound source. Harmonics affect the SNR of the impulse response, but if the impulse response is calculated by inversely filtering the response to the Swept-Sine signal, the harmonic components can be separated. In particular, it is easy to separate in the Log-SS [43]. However, this approach avoids the effect of nonlinearity only if the measurement system can be modeled as a memoryless nonlinearity followed by a nonlinear filter. This means that it is only possible to model it as a Hammerstein filter [51]. Therefore, Carini et al. modeled the entire measuring chain (power amplifier, loudspeaker, acoustic path, microphone) as a Legendre nonlinear (LN) Filter [52]. This filter Perfect periodic siquences(PPSs) uses the inputs to estimate the coefficients of the LN filter and calculates the cross-correlation between the system outputs and the basis functions. PPSs is a periodic sequence that guarantees the perfect orthogonality of the basis functions over the sequence duration [53]. Furthermore, this approach has been extended to the Wiever nonlinear (WN) filter [54]. These papers demonstrate the robustness of the filter proposed by experiments to the nonlinearity of room acoustic measurements. Still more robust systems against nonlinearity are still under study [55]. It is inferred that the nonlinearity of the sound source, which becomes a problem when attempting to apply LIB to room acoustic measurement in this way, can be eliminated by considering the filtering applied when calculating the impulse response from the measurement signal and measurement results.

7.2 Combination with spatial audio

The combination of aerial video and acoustics can be substituted by leaving the acoustic part to stereoscopic sound and synchronizing the position of the aerial video with the sound image presented by stereoscopic sound. The generation of LIB can be left to a laser of higher power by sharing the role in this way in the case of the purpose of art expression, since the focal length can be lengthened, it is possible to produce an effect utilizing the advantages of both. It is necessary to investigate how the user experience changes when sound images are combined with aerial images, and when sound is generated from aerial images themselves. If there is no significance in the technique for producing sound from aerial images, it is better to use a combination of stereoscopic sound systems that can provide stable reproduction

even in the low-frequency range where the LIB is difficult to reproduce.

7.3 Frequency shift by moving focus

The frequency of the sound that is generated when the LIB is moved varies. You should identify the cause of this problem and correct it during the modulation or playback phase. The Doppler effect is commonly known to occur when the frequency of a moving sound source changes. The frequency shift of the LIB may also be a Doppler-like phenomenon. In order to solve this problem, it is expected that the moving speed of the focus and the frequency characteristics of the sound to be played back must be changed. Detailed analysis and implementation of solutions are future challenges. Using this phenomenon, audibility can also be generated using a high-speed scannable galvanomirror [8]. In this modulation method, the focal length of the lens needs to be long to some extent, and since the sound source position fluctuates, it is necessary to thoroughly examine how much omnidirectional it should be kept. Since there is no potential noise present in pulse-modulation, the development of a high-speed MEMS mirror that can accommodate high output can lead to higher sound quality sound source reproduction.

7.4 Size of workspace

LIB can be positioned freely in the air by moving the focus position, but the size of the workspace is ultimately limited to the objective that focuses the laser beam. Larger workspaces require objective lenses with larger apertures. Ochiai et al. moves the generating point of LIB by mirrors to the galvo and expresses the aerial image [5]. The use of lenses with large numerical apertures and large diameters allows for a wider range of XY scans, which extends the potential for more flexible spatial placement and application applications. The distance from the lens to the LIB depends on the focal length of the lens, but if a lens with a long focal length focuses a high power beam, you should be aware of the formation of the plasma tail by filamenting. By choosing a larger lens diameter and focusing from a wider beam diameter, the focal intensity is shallower and the effect of filamenting can be minimized.

7.5 Acoustic reflection from optical equipment

LIB is a massless sound source and does not reflect any sound. However, lenses and laser bodies used to focus the laser will reflect sound. To avoid this effect, the focal length of the lens used for condensing is increased to separate the acoustic measurement environment from the optical circuit by separating the light-blocking walls such as glass. A necessary factor for increasing the focal length is First, to increase the output of the laser source. Second, use a lens with a high NA. Third, expand the beam diameter to match the lens diameter to take advantage of the NA of the lens. Also, the shorter the pulse width of the laser source, the higher the power concentration.[9]. Since the laser source itself generates operating noise, it is preferable to install the oscillation circuit and cooling device in separate rooms.

7.6 Noise depending on modulation method

Since PFM integrates the swings of the audio waveform data and compares them with the threshold values, it adds a direct current component to the wave data represented by the acquisitions so that there are no negative values. This direct current component generates a peak at a constant frequency when it is integrated. For example, even if a no sound file with a zero amplitude is modified over the entire time period, a certain frequency of noise is added. In this paper, I eliminated the noise by a forcing means to eliminate this noise, but the completely eliminated noise was only the silent part of the beginning part. Using such a forcing method did not obviously adversely affect the characteristics of the audible frequency band, but it is very likely that even the output of the timing at which the pulses should be output has been eliminated as noise. As a sound source reproduction technique, it operates on the same principles as a 1-bit audio format called Direct Stream Digital (DSD). The sampling frequency of the DSD is even higher than the maximum frequency 496kHz used in this paper, and there is a report in the previous study that it felt similar sound quality to the PCM format of 192kHz at a sampling frequency of 5.8MHz [56]. This suggests that the sampling frequency of the system in this paper may not be able to achieve playback with sufficiently high sound quality. Faster switching can only be achieved by using a acousto-optic (AO) device or Electro-Optics (EO) device, but these devices are rarely capable of withstanding high-energy lasers. If a custom-made, high-voltage, high-speed device can be fabricated, it can be used to shift noise to high frequencies. This is an item that needs to be verified in the future. Using AO Modulator (AOM) to generate audible sound is a common technique in the field of photoacoustics. Another experiment is to amplitude-modulate a continuous laser by an AOM to produce an audible sound in water vapor [8]. The lasers used in this paper also use AOM to modulate the repetition frequency. In addition, an experiment in which measurement was performed by changing the repetition frequency resulted in an increase in volume without having a significant effect on the frequency characteristics if the pulse had a long time of hi and multiple pulses were occurring in it. Using this, a pulse train composed of multiple pulses is regarded as one pulse, and the number of pulses is captured as an amplitude value, which may allow sound to be reproduced using the logic of AM modulation. With this method, the noise of the DC component during modulation is raised to the sampling frequency at the center wavelength, so further shifting of the noise to the high frequency can be expected.

7.7 Risk of high power laser

This paper uses laser light sources classified as Class 4 according to the regulations of International Electrotechnical Commission (IEC) 60825-1:2014. Users using the proposed technique should wear glasses with an infrared filter, as direct vision of the laser beam, exposure to the skin, and observation of diffuse reflections can be dangerous. Since the sound and light generated by the LIB are radiated in all directions, the user can observe the phenomenon without interfering with the path of the laser beam. There are several reports of skin damage caused by femtosecond lasers. The minimal visible diseasing thresholds of the pig skin of the pulsed laser were verified by Clarence [57]. Skin surface damage progressed with acoustic effects, laser ablation, and low-density plasma effects, depending

on the wavelength and pulse duration of the femtosecond laser (wavelength 810nm, pulse width 44fs, spot size 12mm). From the observations that the effect of the injury was burnt out in 24 hours after exposure, ED50(effective dose 50%) was determined as 21mJ. Shorter exposure times minimize the impact of damage.

Chapter 8

Conclusion

In this paper, I introduced how to generate plasma (LIB) in air by dielectric breakdown of air with a femtosecond laser (wavelength 1035nm, pulse width 275fs, repetition frequency 1k-1MHz, pulse energy 40μJ/pulse) to realize an aerial speaker capable of reproducing arbitrary waveforms. The created control system electronically controlled the laser shutters by means of pulse patterns obtained by Pulse Frequency modulation sound source files. The characteristics of the sound source generated by LIB were experimented by creating an anechoic chamber and drilling holes for laser light incidence to suppress the effects of noise. The characteristics of the anechoic chamber were evaluated by indoor impulse-response measurements using Swept-Sine signal. The frequency characteristics of the sound reproduced by the LIB measured in the chamber tend to increase toward the high frequency, and the noise of a constant frequency by the modulation method was confirmed. The recorded signal was observed to descend separately from the main signal, which increased in frequency. Since the sound generated by LIB is due to shock waves, it was presumed that it has a property similar to a triangular wave. Compared with the spectrogram of the saw wave actually generated by the software, it was confirmed that it descended similarly. The sound source characteristics were measured by changing the sampling frequency of the sound source. This experiment showed that the lower the sampling frequency, the more dominant the effect of low-frequency noise. This result was inferred from the Fourier series expansion of the saw wave to be a phenomenon that the amplitude becomes smaller at frequencies farther from the center wavelength of the noise. The effect of pulse width on the playback sound changed the energy density per unit time of the laser and affected the volume of the playback sound. In addition, I proposed an application to room acoustics measurement. The nonlinearity of LIB can be avoided by devising a filter used to calculate the signal and impulse response used for measurement. LIB generated by ultrashort pulsed lasers have attracted attention as a potential sound source that meets ISO 3382-1 requirements, and have been considered for measuring room impulse responce (RIRs) using a reduced model as an impulsive sound source. Since signals with improved signal-to-noise ratios such as Swept-sine signal are actually used for measuring RIR, measuring RIR using a reduced model applying the systems proposed in this paper may give more accurate results.

Acknowledgement

First of all, I am deeply grateful to Prof.Yoichi Ochiai, Takayuki Hoshi, Prof.Takahito Aoto, Prof.Yoshio Hayasaki, Kota Kumagai. I was able to grow greatly thanks to the responsibility of the optical equipment. I made many mistakes (e.g. burn the SLM, eventually not using Pockels), but all were very exciting experiences. Prof.Ochiai taught me the interest of research. Thank you for showing me the way of life. Hoshi has been a great helper since my undergraduate years. Prof.Aoto is always gave me inspieation for the implementation. Prof.Yoshio Hayasaki and Kota Kumagai, helps me from Utsunomiya. The implementation of this paper would not have been possible without your advice. Deeply thank you all.

References

[1] Hugo Sobral, Mayo Villagrán-Muniz, Rafael Navarro-González, and Alejandro C. Raga. Temporal evolution of the shock wave and hot core air in laser induced plasma. *Applied Physics Letters*, Vol. 77, No. 20, pp. 3158–3160, 2000.

[2] Christophe Ayrault, Philippe Béquin, and Sophie Baudin. Characteristics of a spark discharge as an adjustable acoustic source for scale model measurements. 04 2012.

[3] Chien-Jen Lai and Franz X. Kärtner. The influence of plasma defocusing in high harmonic generation. *Opt. Express*, Vol. 19, No. 23, pp. 22377–22387, Nov 2011.

[4] Kota Kumagai, Satoshi Hasegawa, and Yoshio Hayasaki. Volumetric bubble display. *Optica*, Vol. 4, No. 3, pp. 298–302, Mar 2017.

[5] Yoichi Ochiai, Kota Kumagai, Takayuki Hoshi, Jun Rekimoto, Satoshi Hasegawa, and Yoshio Hayasaki. Fairy lights in femtoseconds: Aerial and volumetric graphics rendered by focused femtosecond laser combined with computational holographic fields. *ACM Trans. Graph.*, Vol. 35, No. 2, February 2016.

[6] Naoki Hosoya, Masaki Nagata, and Itsuro Kajiwara. Acoustic testing in a very small space based on a point sound source generated by laser-induced breakdown: Stabilization of plasma formation. *Journal of Sound and Vibration*, Vol. 332, No. 19, pp. 4572 – 4583, 2013.

[7] Qin Qin and Keith Attenborough. Characteristics and application of laser-generated acoustic shock waves in air. *Applied Acoustics*, Vol. 65, No. 4, pp. 325 – 340, 2004.

[8] Ryan M. Sullenberger, Sumanth Kaushik, and Charles M. Wynn. Photoacoustic communications: delivering audible signals via absorption of light by atmospheric h2o. *Opt. Lett.*, Vol. 44, No. 3, pp. 622–625, Feb 2019.

[9] Javier Gómez Bolaños, Symeon Delikaris-Manias, Ville Pulkki, Joona Eskelinen, and Edward Hæggström. Laser-induced acoustic point source for accurate impulse response measurements within the audible bandwidth. *The Journal of the Acoustical Society of America*, Vol. 135, No. 6, pp. EL298–EL303, 2014.

[10] E. Manikanta, L. Vinoth Kumar, P. Venkateshwarlu, Ch. Leela, and P. Prem Kiran. Effect of pulse duration on the acoustic frequency emissions during the laser-induced breakdown of atmospheric air. *Appl. Opt.*, Vol. 55, No. 3, pp. 548–555, Jan 2016.

[11] Jeffrey Borish and James B. Angell. An efficient algorithm for measuring the impulse response using pseudorandom noise. *J. Audio Eng. Soc*, Vol. 31, No. 7/8, pp. 478–488, 1983.

[12] Nobuharu Aoshima. Computer- generated pulse signal applied for sound measurement. *The Journal of the Acoustical Society of America*, Vol. 69, No. 5, pp. 1484–1488, 1981.

[13] R. W. Rochelle. Pulse-frequency modulation. *IRE Transactions on Space Electronics and Telemetry*, Vol. SET-8, No. 2, pp. 107–111, June 1962.

[14] T. Tajima and J. M. Dawson. Laser electron accelerator. *Phys. Rev. Lett.*, Vol. 43, pp. 267–270, Jul 1979.

[15] L. V. KELDYSH. IONIZATION IN THE FIELD OF A STRONG ELECTROMAGNETIC WAVE. Vol. 20, No. 5, pp. 1307–1314, 1965.

[16] Miłosz Pawlicki, HazelA. Collins, RobertG. Denning, and HarryL. Anderson. Two-photon absorption and the design of two-photon dyes. *Angewandte Chemie International Edition*, Vol. 48, No. 18, pp. 3244–3266, 2009.

[17] Jérôme Kasparian and Jean-Pierre Wolf. Physics and applications of atmospheric nonlinear optics and filamentation. *Opt. Express*, Vol. 16, No. 1, pp. 466–493, Jan 2008.

[18] Guozhen Yang and Y. R. Shen. Spectral broadening of ultrashort pulses in a nonlinear medium. *Opt. Lett.*, Vol. 9, No. 11, pp. 510–512, Nov 1984.

[19] Alexander L. Gaeta. Catastrophic collapse of ultrashort pulses. *Phys. Rev. Lett.*, Vol. 84, pp. 3582–3585, Apr 2000.

[20] L. Bergé and A. Couairon. Gas-induced solitons. *Phys. Rev. Lett.*, Vol. 86, pp. 1003–1006, Feb 2001.

[21] Y.R. Shen. Self-focusing: Experimental. *Progress in Quantum Electronics*, Vol. 4, pp. 1 – 34, 1975.

[22] V P Kandidov, O G Kosareva, and Svyatoslav A Shlenov. Influence of transient self-defocusing on the propagation of high-power femtosecond laser pulses in gases under ionisation conditions. *Quantum Electronics*, Vol. 24, No. 10, pp. 905–911, oct 1994.

[23] Effy Wille, Miguel Rodriguez, Jérôme Kasparian, Didier Mondelain, Jiance yu, André Mysyrowicz, Roland Sauerbrey, Jean-pierre Wolf, and Ludger Woeste. Teramobile: A mobile femtosecond-terawatt laser and detection system. *http://dx.doi.org/10.1051/epjap:2002090*, Vol. 20, , 12 2002.

[24] A. Brodeur, C. Y. Chien, F. A. Ilkov, S. L. Chin, O. G. Kosareva, and V. P. Kandidov. Moving focus in the propagation of ultrashort laser pulses in air. *Opt. Lett.*, Vol. 22, No. 5, pp. 304–306, Mar 1997.

[25] John F. Ready. *Industrial Applications of Lasers. SECOND EDITION.* Academic Press, 2nd edition.

[26] "Barbara Kaltenbacher". "mathematics of nonlinear acoustics". *"Evolution Equations Control Theory"*, Vol. "4", No. "2163-2480$_2$015$_{44}$47", *p.*"447", "2015"."".

[27] Don A. Webster and David T. Blackstock. Finite- amplitude saturation of plane sound waves in air. *The Journal of the Acoustical Society of America*, Vol. 62, No. 3, pp. 518–523, 1977.

[28] Masahide Yoneyama, Jun- ichirohFujimoto, Yu Kawamo, Shoichi Sasabe. The audio spotlight: An application of nonlinear interaction of sound waves to a new type of loudspeaker design. *The Journal of the Acoustical Society of America*, Vol. 73, No. 5, pp. 1532–1536, 1983.

[29] Yoichi Ochiai, Takayuki Hoshi, and Ippei Suzuki. Holographic whisper: Rendering audible sound spots in three-dimensional space by focusing ultrasonic waves. In *Proceedings of the 2017 CHI Conference on Human Factors in Computing Systems*, CHI '17, p. 4314–4325, New York, NY, USA, 2017. Association for Computing Machinery.

[30] W. R. Babcock, K. L. Baker, and A. G. Cattaneo. Musical flames. *The Journal of the Acoustical Society of America*, Vol. 43, No. 6, pp. 1465–1466, 1968.

[31] Naoki Teraguchi and Masataka Minami. Development of musical solid-state tesla coil based on pulse repetition frequency method. *Electronics and Communications in Japan*, Vol. 102, No. 8, pp. 11–16, 2019.

[32] Olaf Bölke, Deanna A Lacoste, and Jonas P Moeck. Low-frequency sound generation by modulated repetitively pulsed nanosecond plasma discharges. *Journal of Physics D: Applied Physics*, Vol. 51, No. 30, p. 305203, jul 2018.

[33] Wayne M. Wright and Nicholas W. Medendorp. Acoustic radiation from a finite line source with n- wave excitation. *The Journal of the Acoustical Society of America*, Vol. 43, No. 5, pp. 966–971, 1968.

[34] F Bastien. Acoustics and gas discharges: applications to loudspeakers. *Journal of Physics D: Applied Physics*, Vol. 20, No. 12, pp. 1547–1557, dec 1987.

[35] Javier Gómez Bolaños, Ville Pulkki, Pasi Karppinen, and Edward Hæggström. An optoacoustic point source for acoustic scale model measurements. *The Journal of the Acoustical Society of America*, Vol. 133, No. 4, pp. EL221–EL227, 2013.

[36] Joona Eskelinen, Edward Hæggström, Symeon Delikaris-Manias, Javier Gómez Bolaños, and Ville Pulkki. Beamforming with a volumetric array of massless laser spark sources—application in reflection tracking. *The Journal of the Acoustical Society of America*, Vol. 137, No. 6, pp. EL389–EL395, 2015.

[37] Marc Ressl and Pablo Wundes. Design of an acoustic anechoic chamber for application in hearing aid research. 06 2010.

[38] Tor Erik Vigran. *Building Acoustics*. Taylor & Frncia Group, 2008.

[39] K.B.Ginn and M.Sc. *Architectural Acoustics*. Briiel & Kjaer, 1978.

[40] D. Vigé. 13 - vehicle interior noise refinement – cabin sound package design and development. In Xu Wang, editor, *Vehicle Noise and Vibration Refinement*, pp. 286 – 317. Woodhead Publishing, 2010.

[41] *Nature and Phase Properties of Unsaturated Soil*, chapter 2, pp. 29–79. John Wiley Sons, Ltd, 2012.

[42] Nikolaos M. Papadakis and Georgios Stavroulakis. Review of acoustic sources alternatives to a dodecahedron speaker. *Applied Sciences*, Vol. 9, p. 3705, 09 2019.

[43] Angelo Farina. Simultaneous measurement of impulse response and distortion with a swept-sine technique. In *Audio Engineering Society Convention 108*, Feb 2000.

[44] Hirokazu Ochiai and Yutaka Kaneda. Impulse response measurement with constant signal-to-noise ratio over a wide frequency range. *Acoustical Science and Technology*, Vol. 32, No. 2, pp. 76–78, 2011.

[45] Yuki Nakahara and Yutaka Kaneda. Effective measurement method for reverberation time using a constant signal-to-noise ratio swept sine signal. *Acoustical Science and Technology*, Vol. 36, No. 4, pp. 344–346, 2015.

[46] Eiji Takahashi, Pengfei Lan, Oliver Mücke, and Yasuo Nabekawa. Attosecond nonlinear optics using gigawatt-scale isolated attosecond pulses. *Nature communications*, Vol. 4, p. 2691, 10 2013.

[47] Yuxi Fu and Eiji Takahashi. Towards a petawatt-class few-cycle infrared laser system via dual-chirped optical parametric amplification. *Scientific Reports*, Vol. 8, , 12 2018.

[48] F. Baumgarte and C. Faller. Binaural cue coding-part i: psychoacoustic fundamentals and design principles. *IEEE Transactions on Speech and Audio Processing*, Vol. 11, No. 6, pp. 509–519, Nov 2003.

[49] K. Hamasaki, T. Nishiguchi, R. Okumura, Y. Nakayama, and A. Ando. A 22.2 multichannel sound system for ultrahigh-definition tv (uhdtv). *SMPTE Motion Imaging Journal*, Vol. 117, No. 3, pp. 40–49, April 2008.

[50] Yutaro Sugibayashi, Sota Kurimoto, Daisuke Ikefuji, Masanori Morise, and Takanobu Nishiura. Three-dimensional acoustic sound field reproduction based on hybrid combination of multiple parametric loudspeakers and electrodynamic subwoofer. *Applied Acoustics*, Vol. 73, No. 12, pp. 1282 – 1288, 2012. Parametric Acoustic Array: Theory, Advancement and Applications.

[51] Thomas Schmitz and Jean-Jacques Embrechts. Hammerstein kernels identification by means of a sine sweep technique applied to nonlinear audio devices emulation. *J. Audio Eng. Soc*, Vol. 65, No. 9, pp. 696–710, 2017.

[52] A. Carini, S. Cecchi, L. Romoli, and G. L. Sicuranza. Perfect periodic sequences for legendre nonlinear filters. In *2014 22nd European Signal Processing Conference (EUSIPCO)*, pp. 2400–2404, Sep. 2014.

[53] Christiane Antweiler. *Multi-Channel System Identification with Perfect Sequences – Theory and Applications* –, chapter 7, pp. 171–198. John Wiley Sons, Ltd, 2008.

[54] A. Carini, S. Cecchi, A. Terenzi, and S. Orcioni. On room impulse response measurement using perfect sequences for wiener nonlinear filters. In *2018 26th European Signal Processing Conference (EUSIPCO)*, pp. 982–986, Sep. 2018.

[55] A. Carini, S. Orcioni, and S. Cecchi. On room impulse response measurement using orthogonal periodic sequences. In *2019 27th European Signal Processing Conference (EUSIPCO)*, pp. 1–5, Sep. 2019.

[56] Atsushi Marui, Toru Kamekawa, K. Endo, and E. Sato. Subjective evaluation of high resolution recordings in pcm and dsd audio formats. *136th Audio Engineering Society Convention 2014*, pp. 104–113, 01 2014.

[57] Clarence P. Cain, William P. Roach, David J. Stolarski, Gary D. Noojin, Semih S. Kumru, Kevin L. Stockton, Justin J. Zohner, and Benjamin A. Rockwell. *Infrared laser damage thresholds for skin at wavelengths from 0.810 to 1.54 microns for femto-to-microsecond pulse durations*, Vol. 6435 of *Society of Photo-Optical Instrumentation Engineers (SPIE) Conference Series*, p. 64350W. 2007.